6-24-2008

Detection of Marine Vehicles in Images and Video of Open Sea

Sergiy Fefilatyev
University of South Florida

Detection of Marine Vehicles in Images and Video of Open Sea

by

Sergiy Fefilatyev

A thesis submitted in partial fulfillment
of the requirements for the degree of
Master of Science in Computer Science
Department of Computer Science and Engineering
College of Engineering
University of South Florida

Major Professor: Dmitry B. Goldgof, Ph.D.
Lawrence O. Hall, Ph.D.
Sudeep Sarkar, Ph.D.

Date of Approval:
June 24, 2008

Keywords: ship detection, tracking, horizon detection, computer vision, buoy camera,
Kalman filter, machine learning, performance evaluation

DEDICATION

This thesis is dedicated to my parents, Larisa and Nikolay Fefilatyev, for support during my academic years.

ACKNOWLEDGEMENTS

I would like to express words of sincere gratitude to my major professor Dr. Dmitry Goldgof for giving me opportunity to work in the field of computer vision under his supervision. Thank you, Dr. Lawrence Hall and Dr. Sudeep Sarkar, for assisting me during the years of graduate school and providing constant scientific input and feedback. I would also like to extend my gratitude to Mr. Larry Langebrake and Mr. Chad Lembke from the Center of Ocean Technology for giving the idea for the project, consulting in the field of marine science and providing image and video data for experimental work.

TABLE OF CONTENTS

LIST OF TABLES

LIST OF FIGURES

DETECTION OF MARINE VEHICLES IN IMAGES AND VIDEO OF OPEN SEA

Sergiy Fefilatyev

ABSTRACT

This work presents a new technique for automatic detection of marine vehicles in images and video of open sea. Users of such system include border guards, military, port safety, flow management, and sanctuary protection personnel. The source of images and video is a digital camera or a camcorder which is placed on a buoy or stationary mounted in a harbor facility. The system is intended to work autonomously, taking images of the surrounding ocean surface and analyzing them for the presence of marine vehicles. The goal of the system is to detect an approximate window around the ship. The proposed computer vision-based algorithm combines a horizon detection method with edge detection and postprocessing. Several datasets of still images are used to evaluate the performance of the proposed technique. For video sequences the original algorithm is further enhanced with a tracking algorithm that uses Kalman filter. A separate dataset of 30 video sequences 10 seconds each is used to test its performance. Promising results of the detection of ships are discussed and necessary improvements for achieving better performance are suggested.

CHAPTER 1

INTRODUCTION

1.1 Overview

Ship monitoring is an essential process for a number of applications of practical importance. It is utilized by border guards and military, is an important element in securing ports and sanctuary protection. This work presents an algorithm for an automated computer system that detects ships on the horizon. Such a system can be equipped with a digital camera, located on a buoy or stationary mounted in a port facility and will work in an autonomous mode taking images of the surrounding area. After processing the image information the system would only send images of the found objects to a human operator for further evaluation and action (see Figure 1.1).

The objective of this prototype system lies in effective detection of the presence of ships on the horizon, isolating ships in the image and preparing an image-result to be transmitted to a control center for a review by a human evaluator. One of the constraints for such a system is the low communication bandwidth available while reporting the results. Hence, one of the requirements lies in efficient compression of the obtained visual results before they are sent to the control center. Another constraint is low power consumption. The latter requirement suggests that algorithms utilized by the system should have minimum complexity while processing image data. This work describes software system components that comprise basic algorithm for detecting ships in images of the open sea taken by a digital camera. Relationships between these components is discussed and the performance of the algorithm is shown on two datasets of still images: (a) 100 independent images with multiple ships present; (b) a dataset consisting of 9000 frames from 30 video sequences. In order to enhance results on video data a tracking algorithm is introduced and its per-

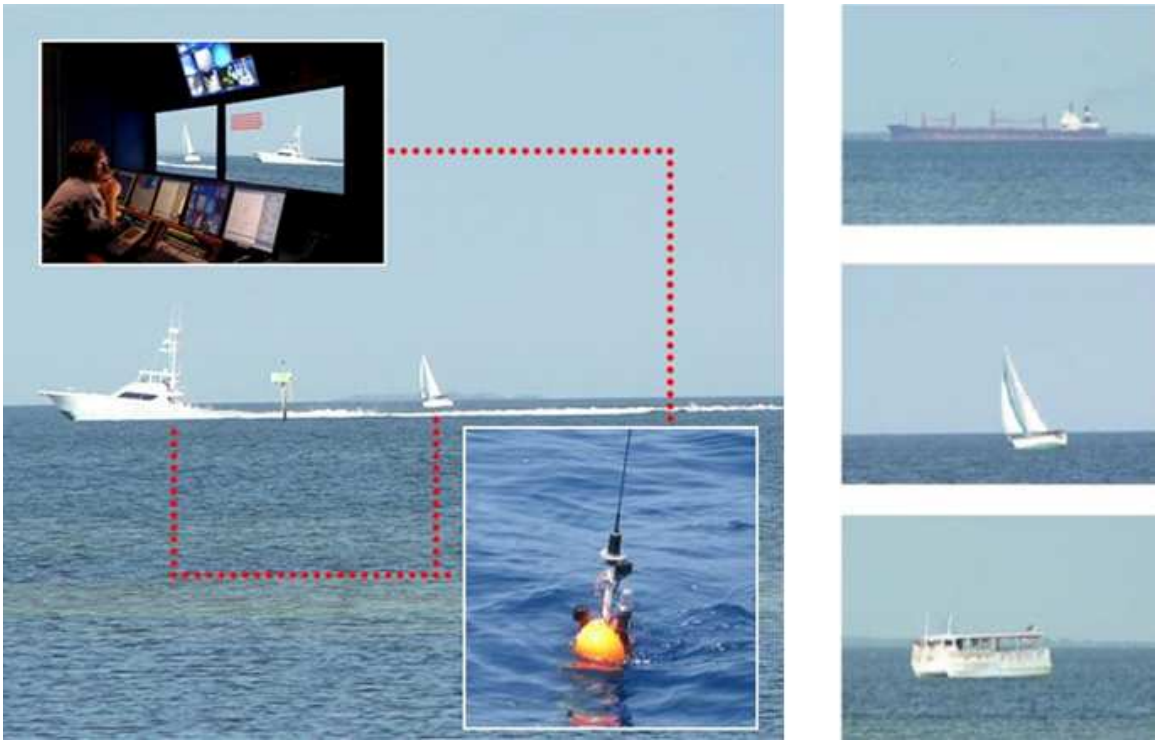

Figure 1.1. Proposed buoy-based sea-traffic monitoring system.

formance is shown. In summary some improvements for more reliable and robust marine vessel detection algorithm are suggested.

1.2 Previous Work

1.2.1 Marine Vehicles Detection

Most of the job in sea monitoring is done using radio radars [1]. They rely on reflection of electromagnetic waves from a change in the dielectric or diamagnetic constants. A radar transmitter emits radio waves, which are reflected by the target. Reflected radio waves are detected by a radar receiver. Target objects are detected based on the latency between transmitted and received signals. A range of objects, including weather formations, ground and sea surfaces reflect radio waves and, thus, may be detected. However, the radio reflection is particularly high for electrically conductive materials, such as metal and carbon fiber, the material widely used for frames of the marine vessels and aircraft.

Radar's ability to detect metal objects of various sizes depends on the choice of operating frequency. High (microwave) frequency marine radars are employed in most of the current vessels, aircraft and ground stations for ships detection. They have properties of reliable detection of even relatively small (with radar cross section of about 1 m^2 objects. However, the operating range of those radars is limited by linear distance to the target objects and usually does not exceed 10-20 miles or more for airborne installed systems.

Another category of radars, ground wave over-the-horizon radars (GWOTHR), use lower frequencies of radio waves, and thus, can propagate signal along the curved surface. They also use the fact of refraction of radio waves in ionosphere. This provides GWOTHR radars with surveillance capabilities over very large areas. For example [2] reports results for technical capabilities of Northern Radar's Cape Race Ground Wave Radar system which had the potential to provide surveillance of over 160,000 square kilometers. Its range of targets included ships, icebergs, as well as environmental parameters such as surface currents and sea states. This category of radars is able to detect low-flying aircraft on big distances but detection of marine vehicles on big distances is limited to due the small radial Doppler velocity of the vessels: the targets' Doppler usually shares the same spectral region with the continuum of high order sea clutter [3].

Another approach to ship detection is described in [4]. This method uses magnetic fields around magnetic targets to detect relatively large ships on the surface or even submarines in a submerged state. A magnetometer onboard an aircraft measures anomalies in the magnetic field in the area surrounding the aircraft. Although conceptually proven to detect artificial metal objects, this exotic method, however, is more suitable for geology, for finding deposits of iron ore or other metal resources. Detection of sea target is limited by the distance from magnetometer to the target. The nature of magnetic field requires the aircraft carrying the system to be in the close vicinity to the target.

The next category of radars, SAR (Synthetic Aperture Radar) has many applications in remote sensing and mapping. The approach uses sophisticated postprocessing of radar data to produce a very narrow effective microwave beam [5]. SAR can only be used on moving platforms to conduct sensing over relatively immobile targets. The two most

used platforms for SAR are satellites (for spaceborne SAR) or aircraft (for airborne SAR). Marine vehicles and coast line detection by SAR has become a topic of considerable interest since the upsurge of demand for this kind of information in the commercial market. SAR capabilities include all weather and all day detection, high resolution and wide coverage (around 100x100 km). The result of sensing using the radar is an image of the ocean surface. Current systems used for ship detection vary in the computer vision approaches to detect the objects of interest. Many techniques [6], [7] search for features of the wake of a ship in a SAR image. In [8] the Radon transform of SAR images of ship wakes and ocean waves was computed and an enhancement operator within the transform space was applied.

In more advanced work using SAR images instances of ships are assigned a class or category (i.e. destroyer, aircraft carrier). In [9] radar images were used to classify ships based on global features. Morphological analysis of the object boundary from SAR images was utilized in [10]. Classification of the ships and their motion parameters is described in [11] and [12].

Other imaging sensors were used for ship detection as well. Forward Looking Infra Red (FLIR) cameras is often a good sensor of choice because the images they provide are insensitive to lighting conditions. This imaging sensor is more desirable in military applications because it does not reveal the location of the imaging system. Many approaches can be found the in the literature for ship classification in FLIR images. In [13] they used the principal component global features and similarity matching to classify ship silhouettes. The authors of [14] used neural networks applied directly to image pixels. Recent work on ship classification in [15] uses a k Nearest Neighbor classifier on shape features extracted with MPEG-7 region-based shape descriptor.

A notable disadvantage of FLIR systems is the low resolution of the images obtained which requires a relatively small viewing distance of the imaging system to the target. It is also more power consuming and, thus, is less capable for autonomous operation. The approach described in [16] uses solely computer vision algorithms and image data from regular digital cameras (in the visual spectrum) to detect marine vehicles. It is

aimed for autonomous operation, under power and communication bandwidth constraints. The applications for its use include local sea traffic monitoring in sanctuaries and port zones. Images of open sea taken from a forward looking camera installed on a buoy. After detecting horizon line the system looks for objects lying on it. The system is intended to monitor only local traffic, within visible distance. However, the absence of radars and reliance on simple computer vision algorithms makes the potential system cheap and easy in deployment and maintenance. This document enhances preliminary results described in [16]. It adds additional robustness to horizon detection for single images. It also uses tracking techniques to improve detection in video sequences.

1.2.2 Horizon Detection

Another category of related work that should be mentioned includes horizon detection in images. Accurate horizon detection gets considerable attention in this thesis. According to the literature survey performed for this work most of horizon detection approaches were designed for navigation of micro air vehicles (MAV). While larger aircraft may have high-precision gyros to sense angular rates or acceleration, smaller MAV have very strict constraints for payload capacity, dimensions, and electrical power. MAV autonomous flight control system in many cases relies on cheap and light on-board imaging sensors such as cameras, which, however, provide rich information content. In addition to surveillance tasks that have been considered as the primary mission of MAV, such imaging sensors allow estimation of navigation parameters. Pitch angle and roll angle of a MAV can be extracted based on the horizon line in the video images. Several vision systems have been reported to provide vision-based horizon-tracking.

One research group, very active in vision-based navigation, has published a number of papers related to horizon detection [17, 18, 19, 20]. Their basic approach, a statistical horizon detection algorithm, attempts to minimize the intra-class variance of the ground and sky distribution. The horizon is considered a line with high likelihood of separating the sky from ground (or non-sky) regions.

Other approaches developed by different authors [21, 22] rely on more simple and less computationally intensive algorithms. The horizon angle is found as a function of the average coordinates for sky and non-sky classes. The angle of the horizon is determined by taking the perpendicular of the line joining sky and non-sky centroids. Sky and non-sky regions are distinguished by a simple thresholding criterion based on the brightness of pixels in a grayscale image.

A considerably different technique is described in [23]. It uses an idea similar to skew detection in document image analysis, i.e. detecting the skew of the scanned documents. The original image is preprocessed and edges are extracted. Projection profiles of edges in the image for different angles are obtained and the horizon is found in the profile corresponding to the largest peak of such a projection.

The approach described in [24] was designed not only for horizon detection but also to avoid obstacles during MAV flights. The authors classify regions in the image into sky and ground/obstacles and obtain boundaries of the safe area ahead of the aircraft as well as angular parameters of the aircraft determined from the horizon line. Another classification approach, not related directly the MAV navigation, is described in [25]. The horizon is modeled as a line separating sky and non-sky pixel and is found after image content is classified using numerous features into two classes - sky and non-sky.

Several other works related to MAV navigation report more integration with hardware, often allowing on-board processing of the data. One research group developed horizon detection equipment that is light enough to be airborne [26]. They use a thermal imaging camera and scanned linear array. Similar approaches that use the infra-red spectrum are used in aerospace application for stabilizing aircraft and are described in [27].

Chapter 5 will continue the discussion about horizon detection optimal needed for this work. The mentioned horizon detection algorithms will be reviewed in more detail and several will be evaluated for performance.

CHAPTER 2

BACKGROUND

2.1 Edge Detection

Edge detection is a research field within image processing and feature extraction and there are many different approaches to it. The goal of edge detection is to mark the points in an image at which the intensity changes sharply. Sharp changes in pixels intensity in an image usually reflect important events and changes in world corresponding to the image. Examples of edge detectors include Sobel, Laplace and Canny and other edge detectors [28], [29], [30]. This work uses Canny edge detector [31].

The algorithm used in Canny's method follows a list of criteria to improve edge detection in comparison to other methods. Its advantages include low error rate, well-localized edge points with minimum distance between the actual edge, and single edge response. The algorithm consists of the following six steps:

- Noise in the original image is filtered out before locating and detecting any edges. Because the Gaussian filter [28], [32] can be computed using a simple mask, it is used exclusively in the Canny algorithm. Once a suitable mask has been calculated, Gaussian smoothing is performed using standard convolution methods.

- The edge strength is found by taking the gradient of the image. 2-D spatial gradient measurement is performed by convolving two (vertical, and horizontal) 3x3 kernels around each pixel in the image. Then, the approximate absolute gradient magnitude (edge strength) at each point can be found. The Sobel operator uses a pair of 3x3 convolution masks, one estimating the gradient in the X direction (columns) and the other estimating the gradient in the Y direction (rows). The magnitude, or edge

strength, of the gradient is then approximated using the formula:

$$|G| = |G_x| + |G_y| \tag{2.1}$$

- Edge direction is found from the gradient magnitude in the X and Y direction using the following formula:

$$\theta = \arctan(\frac{Gx}{Gy}) \tag{2.2}$$

- The non-maximum suppression, used to trace along the edge in the edge direction, is applied after the edge directions are known. This results in a thin line in the output image.

- Hysteresis is used as a means of eliminating streaking. Streaking is the breaking up of an edge contour caused by the operator output fluctuating above and below the threshold. If a single threshold, T1 is applied to an image, and an edge has an average strength equal to T1, then due to noise, there will be instances where the edge dips below the threshold. Equally it will also extend above the threshold making an edge look like a dashed line. To avoid this, hysteresis uses two thresholds, high (T1) and low (T2). Any pixel in the image that has a value greater than T1 is presumed to be an edge pixel, and is marked as such immediately. Then, any pixels that are connected to this edge pixel and that have a value greater than T2 are also selected as edge pixels.

2.2 Connected Components Algorithm

Extracting and labeling of various disjoint and connected components in an image is an important postprocessing step of ship detection. The connected components labeling algorithm [33] is applied on a binary image to group its pixels into components based on pixel connectivity, i.e., all pixels in a connected component share similar pixel intensity values (zero or one) and are in some way connected with each other. Once all groups

have been determined, each pixel is labeled with a number according to the component it was assigned to. The algorithm works by scanning an image, pixel-by-pixel (from top to bottom and left to right) in order to identify regions of adjacent pixels which share the same set of intensity values V.

Connected component labeling works on binary images and two different measures of connectivity are possible: 4-connectivity and 8-connectivity, depending on the number of neighbor pixel possible for connection. For the current project 8-connectivity is used, however, for the purpose of simplicity only 4-connectivity is described here. The labeling operator scans the image by moving along a row until it comes to a point p, where p denotes the pixel to be labeled at any stage in the scanning process for which $V = 1$. When this is true, it examines the four neighbors of p which have already been encountered in the scan (i.e. the neighbors (I) to the left of p, (II) above it, and (III and IV) the two upper diagonal terms). Based on this information, the labeling of p occurs as follows:

- if all four neighbors are 0, assign a new label to p, else
- if only one neighbor has $V = 1$, assign its label to p, else
- if more than one of the neighbors have $V = 1$, assign one of the labels to p and make a note of the equivalences.

The equivalent label pairs after completing the scan are sorted into equivalence classes and a unique label is assigned to each class. As a final step, a second scan is made through the image, during which each label is replaced by the label assigned to its equivalence classes. For display, the labels might be different gray levels or colors.

2.3 Kalman Filter

The Kalman filter [34], [35] provides a recursive solution to the linear optimal filtering problem. Its domain of its applications includes stationary and non-stationary environments. The solution is recursive; each updated estimate of the state is computed from the previous estimate and the new input data. The Kalman filter needs to store only the pre-

vious estimate, eliminating the need for storing the entire past observed data, and, thus is computationally more efficient than computing the estimate from the entire past observed data at each step of the filtering process.

The block diagram shown in Figure 2.1 describes a linear, discrete-time dynamic system. The state vector, denoted by x_k, is defined as the minimal set of data that uniquely describes the unforced dynamical behavior of the system; the subscript k denotes discrete time. The state vector is the least amount of data on the past behavior of the system that is sufficient to predict its future behavior. On general, the state x_k is unknown. To estimate it, a set of observed data, denoted by the vector y_k, is used. Process noise w_k and measurement noise v_k, shown in the diagram, are represented by covariance matrices Q and R, and are considered constant. The following set of equations describes the dynamic system mathematically:

- Process equation

$$x_{k+1} = F_{k+1,k}x_k + w_k \tag{2.3}$$

  where $F_{k+1,k}$ is the transition matrix, which relates the state x_k from time k to time $k+1$ in the absence of noise. The process noise w_k is assumed to be additive, white, with normal probability. Its probability distribution has zero mean with a covariance matrix defined by

$$E[w_n {w_k}^T] = \begin{cases} Q_k & \text{for } n = k \\ 0 & \text{for } n \neq k \end{cases} \tag{2.4}$$

  where T denotes matrix transposition. The dimension of the state space is denoted by m.

- Measurement equation

$$y_k = H_k x_k + v_k \tag{2.5}$$

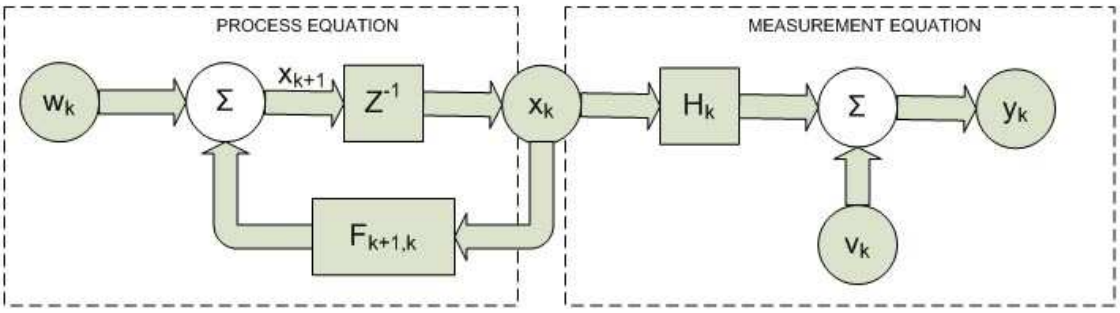

Figure 2.1. Signal-flow graph representation of a linear discrete-time dynamical system.

where y_k is the observable at time k and H_k is the measurement matrix. The measurement noise v_k is assumed to be additive, white, and normal probability. Its probability has zero mean and with covariance matrix defined by

$$E[v_n {v_k}^T] = \begin{cases} R_k & \text{for } n = k \\ 0 & \text{for } n \neq k \end{cases} \tag{2.6}$$

The measurement noise v_k is uncorrelated with the process noise w_k. The dimension of the measurement space is denoted by n.

The Kalman filtering problem, namely, the problem of jointly solving the process and measurement equations for the unknown state in an optimum manner may now be formally stated as follows: use the entire observed data, consisting of the vectors y_1, y_2, ..., y_k, to find for each $k \geq 1$ the minimum mean-square error estimate of the state x_k . The problem is called filtering if $i = k$, prediction if $i > k$ and smoothing if $1 \leq i \leq k$. Detailed techniques for solving Kalman filter problem is shown in [34].

2.4 Texture in Images

The concept of texture is often used to describe region properties in an image. Texture provides measures for properties for a region in an image such as smoothness, coarseness, and regularity and is scale dependant. Texture consists of texture primitives - texture

elements. The three most used approaches to describe the texture of a region in an image are statistical, structural and spectral. Statistical approaches show characterizations of textures as smooth, coarse, grainy, and so on. Structural techniques deal with the arrangement of texture elements, such as the description of texture based on regularity spaced parallel lines. Spectral techniques are based on properties of the Fourier spectrum and are used primarily to detect global periodicity in an image by identifying high energy or peaks in the spectrum.

Because of their simplicity in describing texture this project uses statistical approaches. Those include statistical moments of the gray level histogram, uniformity and entropy calculated for a small region in an image. Let z be a random variable denoting gray levels and let $p(z_i)$, $i = 0, 1, 2, \ldots, L-1$, be the corresponding histogram, where L is the number of distinct gray levels. The nth moment of z, about the mean is

$$\mu_n(z) = \sum_{i=0}^{L-1} (z_i - m)^n p(z_i) \tag{2.7}$$

where m is the mean value of z (the average gray level):

$$m = \sum_{i=0}^{L-1} z_i p(z_i) \tag{2.8}$$

The second moment $\sigma^2(z)$ is a measure of gray level contrast that can be used to establish descriptors of relative smoothness. For example, the measure

$$R = 1 - \frac{1}{1 + \sigma^2(z)} \tag{2.9}$$

is 0 for areas of constant intensity (the variance is zero there) and approaches 1 for large values of $\sigma^2(z)$. Because variance values tend to be large for grayscale images with values, it is normalized to the interval [0,1] for use in (2.9). This is done by simply dividing $\sigma^2(z)$ by $(L-1)^2$ in (2.9). The standard deviation, $\sigma(z)$, also is used frequently as a measure of texture because values of the standard deviation tend to be more intuitive to many people.

The third moment,

$$\mu_3(z) = \sum_{i=0}^{L-1} (z_i - m)^3 p(z_i) \tag{2.10}$$

is related to the skewness of the histogram while the fourth moment is a measure of its relative flatness. The fifth and higher moments are not so easily related to histogram shape, but they do provide further quantitative discrimination of texture content.

Some useful measures based on histograms include a measure of uniformity given by

$$U = \sum_{i=0}^{L-1} P^2(z_i), \tag{2.11}$$

and an average entropy measure, which is defined as

$$e = -\sum_{i=0}^{L-1} p(z_i) \log_2 p(z_i) \tag{2.12}$$

Because the probabilities have values in the range [0,1] and their sum equals 1, the measure U is maximum for an image in which all gray levels are equal (maximally uniform), and decreases from there. Entropy is a measure of variability and is 0 for a constant image.

In general coarse textures are built from larger primitives (texture elements), fine textures have smaller primitives. Coarse textures are characterized by lower spatial frequencies, fine texture by higher spatial frequencies.

Figure 2.2 illustrates different texture measures. For each of the texture measures a texture image of the resolution 256x192 has been received. The method of getting these texture images is the following:

- Obtain a patch of an original image with the size of 11x11 around each pixel in the grayscale image obtained from the original color image.
- Calculate a texture measure for this patch according to (2.7)-(2.12).
- Assign the result of the texture measure as a value of the pixel in the texture image.

- Normalize all values in the texture image equally in the range between 0 and 255.

Thus, for a grayscale image obtained from an original image there are six texture images.

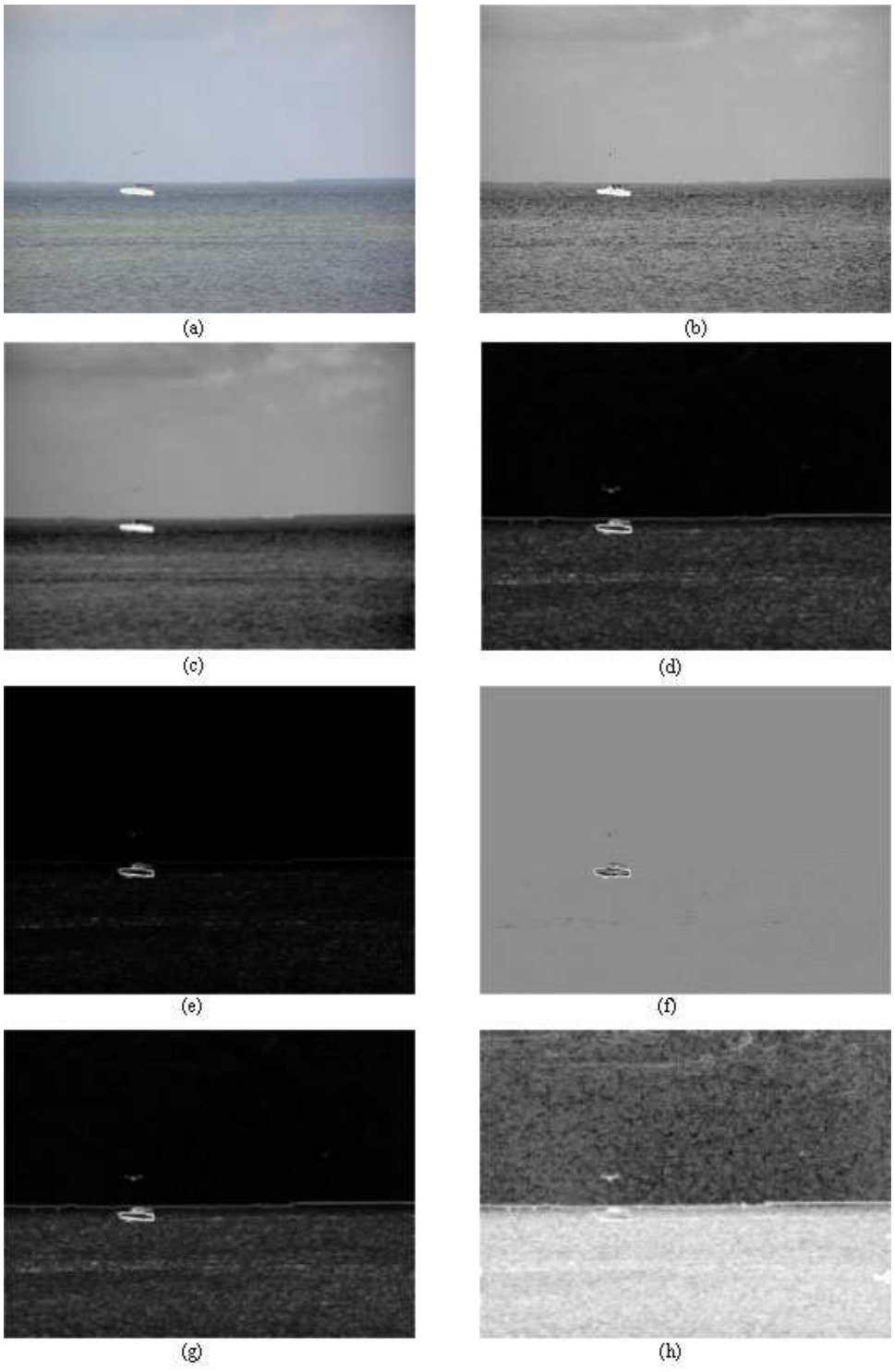

Figure 2.2. Texture images. (a) original color image; (b) corresponding grayscale image of the red channel; (c) texture image using mean measure; (d) texture image using standard deviation measure; (e) texture image using smoothness measure; (f) texture image using third moment measure; (g) texture image using uniformity measure; (h) texture image using entropy measure.

CHAPTER 3

ALGORITHMS

3.1 Overview

The literature section of this document described various methods for detection marine vehicles. These methods differ in technological approaches and potential capabilities. However, most of them are similar in one important aspect: most of these methods are characterized by the high cost of the equipment and maintenance. This creates a very narrow category of users for such systems. In addition, rapid deployment of such systems for monitoring purposes of local areas is difficult, it may require a radar installation or access to satellite data.

This work focuses on detection of marine vehicles using imaging sensor such as digital cameras or camcorders. The scope of surface area for monitoring is limited by visual distance from some point in the ocean or shore. This may be be appropriate for some tasks such as port security or sanctuary protection. In essence, the limitation and effectiveness of the approach are similar to periscope of a submarine: marine vehicles are visually located in image data obtained from a camera sticking out of the water surface. An ocean buoy is considered a primary platform for such a system. An example of appropriate platform can be shown on BSOP - the Bottom Stationing Ocean Profiler [36]. It is an autonomous bouy-platform designed to carry a sensor payload, collect oceanic data and store or/and transmit the data through a bi-directional RF satellite link to a control center. If equipped with a proposed vision unit such a system could perform visual surveillance for passing sea traffic.

The following sections enhance the previous work on algorithmic solution [16] for such a system. In addition to detection of marine vehicles in single images (Section 3.2) other

settings are explored. Section 3.3 adds robustness to the detection approach for video data. Such important aspects as detection, filtering, and tracking are also described.

3.2 Detection of Marine Vehicles in Single Images

Image segmentation and object detection is a broad topic of research in computer vision. Usually, a particular application requires certain assumptions about the environment and targets for detection. Approaches such as background subtraction or appearance similarity are not appropriate for detection of marine vehicles in images with highly dynamic ocean surface. Our assumption for the problem of marine vehicles detection is a relative position between the sought marine objects and the ocean horizon line. That assumption is valid for the case when images or video taken from the camera with image axis parallel to the ocean surface and when the target marine vehicles are located within visual distance. Such assumptions greatly facilitate localization of marine vehicles or other floating objects in image data. This is because the ocean surface part of the image is rich in information content and is difficult to process in terms of image analysis. On the other hand the sky background, in front of which the sought marine vehicles are expected to be located, is relatively homogeneous in color and has little texture, and thus, is easy to process.

Figure 3.1 shows the basic structure and order of steps in the algorithm to detect marine vehicles in single images. The algorithm consists of six steps. During the image acquisition step image data is obtained. Some preprocessing such as basic noise removal is also done during that step. Preprocessed image is fed into two components - edge detector and horizon detector, to obtain, correspondingly, edges from the original image and the parameters of the horizon line. The postprocessing step of the algorithm combines results from edge and horizon detectors and processes only edges that are located above the horizon line. The connected components block of the algorithm provides the location of the bounding boxes around the found marine vehicles. The output result consists of a region from the original image inside the bounding box around found objects. Figure 3.2 shows a sequence of steps in ships detection on a sample image.

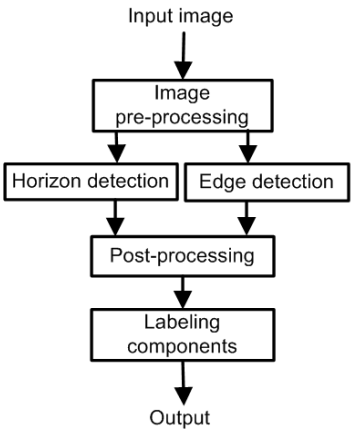

Figure 3.1. Basic structure of ship detection algorithm.

Detailed implementation of the algorithm is described in Subsections 3.2.1–3.2.4.

3.2.1 Image Acquisition

The image acquisition step uses a digital camera installed on a buoy to acquire images of the surrounding area. The image data from the camera is provided in RGB format.The focus of the camera is set to infinity and thus, captures only far-lying objects which are expected to be above the horizon line. The driving factors of such an assumption are the following: at long distances the line between camera and object of interest (a ship) becomes parallel to the sea level and therefore all objects of interest have to exist above the horizon. The height above the water on which the camera is mounted is a matter of consideration. The effective range of detection is bigger when camera is mounted higher. However, a closely located ship may not be exactly above the horizon line detected from such a camera. For some settings the height of camera installation is also a matter of what is practical. For example, buoy systems may not have a mast tall enough to install the camera on the required height. In context of this work the dependency between the height of installation and detection range of the system is not explored. Ideas about the optimal height of the camera-mast for a possible ship surveillance system may be taken from the design of submarine periscope systems [37].

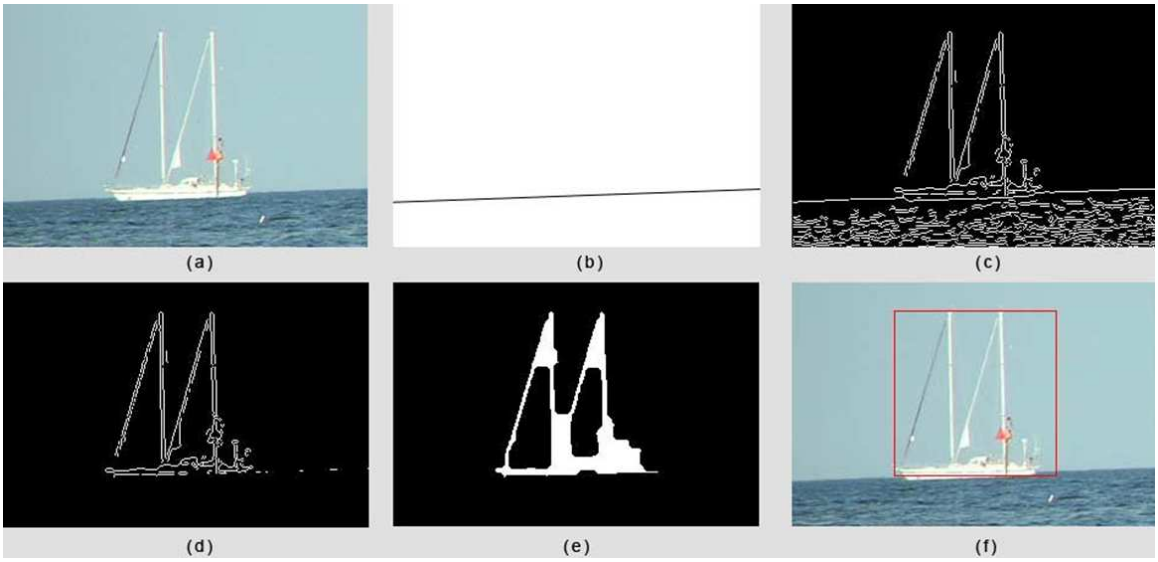

Figure 3.2. Intermediate results during ship detection. (a) Original image. (b) Detected horizon line. (c) Edge-image. (d) Edges taken for consideration (above horizon line). (e) Result of postprocessing step. (f) Bounding box over detected ship.

3.2.2 Edge Detection

The output of this step is a binary map of edges found in the original image. Edges in the images reflect the regions in the images where pixel intensity changes quickly. For a possible marine vehicle with distinct appearance it means sharp changes in intensity at least around the contour of the target in front of sky background. Chapter 2 described the Canny edge detector that was chosen for this work. Good edges should include the contour of a marine vehicles: an edge map that creates a convex hull around the object and exclude edges not belonging to the object. Edges also need to be consistent, possibly having as few broken lines belonging to the same object as possible. The Canny edge detector has three parameters: *sigma* (0.5-5.0), *low* (0.0-1.0) and *high* (0.0-1.0). Automatic search for optimal parameters was not considered in the context of this work because of the difficulties in creating precise pixelwise groundtruth. Manual search for parameters of the Canny edge detector was conducted on a separate dataset of 27 images. The parameters were adjusted to capture only well-defined long edges that are common for vessels with extensive contour

lines like yachts or barges. Figure 3.2 (c) shows an example of edge map detected for original image in Figure 3.2 (a).

3.2.3 Horizon Detection

Horizon detection step is an essential step in the algorithm. The found horizon line is used to eliminate all edges in the edge-map that would not belong to floating objects - we expect that in an image all objects of interest. Failure to identify the horizon correctly results in a lack or abundance of edges that are used in further postprocessing, and consequently, results in incorrect ship identification. Therefore it is very important to choose an algorithm that would provide accurate horizon line detection for different environmental conditions possible in the ocean. Chapter 5 of the thesis presents a detailed analysis of horizon detection algorithms briefly discussed in Chapter 1. It compares different algorithms, shows their performance and describes their advantages and disadvantages for the application of ship detection. Figure 3.2 (d) shows the application of the found horizon line performed in postprocessing step of the algorithm: edges below the horizon line are removed from consideration.

3.2.4 Postprocessing Steps

The purpose of the postprocessing step is to create a preliminary segmentation of objects by creating binary maps where the location of possible target objects is defined by non-zero elements of the map. The input of the step are parameters of the horizon line and a binary edge map from the edge detector. Postprocessing steps zeroes all non-zero elements in the edge map that are located below the horizon line, thus eliminating from results regions of the image where marine vehicles cannot be presents. Since all non-zero pixels are considered to be target pixels it is required to have all pixels that belong to the same object connected. Further in the algorithm connected regions are considered to belong to one object, thus making the discrimination of multiple targets possible.

In order to connect closely lying separate edges belonging to a single object morphology operations of the erosion and dilation are used [28], [32]. Initial use of erosion operation

allows filtering out some small edges that do not belong to target object: parts of uneven horizon line, different objects essential to the ocean environment - flying birds, clouds etc. Further use of erosion and dilation with a bigger structural element allows connection of binary regions that lie within a certain distance relative to the size structural element. The size and shape of the structural element for this work were determined empirically on a test dataset of 27 images. The disk shape was chosen for the structural element. The diameter of the disk was equal to 2 pixels for filtering operations followed by disk with diameter 7 to connect closely lying pixel regions.

3.2.5 Labeling Components and Output

The connected components algorithm (described in Chapter 2) is used to detect bounding boxes around the found objects and groundtruth objects (when performance is evaluated), to find out the size of the objects and to filter out some of the segmentation results.

Every non-zero pixel from the output of the postprocessing step is assigned a label by the connected components algorithm. Pixels that have the same label are connected and belong to one detected object. Thus, this step transforms pixelwise representation of the target to labelwise. By having the pixels of the objects labeled it is possible to check the location of the furthest points of the object in the top, bottom, right, and left sides. Locations of those pixels constitutes the position of the sides the bounding box around the found object. Objects that have intersecting bounding boxes are merged by assigning a single label to the pixels comprising them. After the merge step bounding boxes are computed again and their size is calculated.

All found objects are checked for the proximity to the horizon. Only regions within 10 pixels of the horizon line are further considered to be targets. This operation reduces false alarms caused by birds, clouds, and aircraft which are also located above the horizon line. In the experiment objects which had size less then 6 pixels were eliminated from output. That is justified by the fact that ships in the sea with such small size are less important for a human evaluator and are usually located far enough from the place of interest. Filtering of the small floating objects further reduces false alarm rate when the small regions above

the horizon line represent parts of uneven horizon in the sea, birds on the water surface, etc.

The algorithm outputs the parts of the original image corresponding to the found bounding boxes in connected components step (see Figure 3.2 (f)). Accuracy of detection of marine vehicles is described based on how well the found bounding boxes match groundtruth boxes. Evaluation and performance metrics for such detection are shown in Chapter 4.

3.3 Detection of Marine Vehicles in Video

Such heuristics as vicinity to the horizon line or segmentation techniques greatly reduce the alarm rate and increase the overall accuracy of detection. Still, some steps of the algorithm are prone to errors which cause incorrect results. Example in Figure 3.3 shows one of the typical failures during the horizon detection step. The horizon is detected incorrectly due to a wave surf in the image. The postprocessing step combines edges above the incorrectly detected horizon and considers many more objects for possible targets. Bad performance for ship detection may also stem from the edge detection step when the same object is represented by several disjoint edges. That happens for example when the camera is ill-focused and the image is blurred. In that case the intensity around the contour does not show significant change, edges are not crisp and the edge detector finds only disjoint regions of the same object. Later in the algorithm that may create a miss result for the original ship and false alarm for the attempt. For the example in Figure 3.4 the camera was not focused well enough and the final result was two objects found in the left image and even more in the right image.

Video information allows us to use redundant information to increase the accuracy of ship detection. The assumption used here is that the object present in the current frame should be present in the next frame in close vicinity to the current location. The size of the detected objects should also show consistency between the frames. Sharp changes in the location and size of the objects between the frames may be considered a sign of

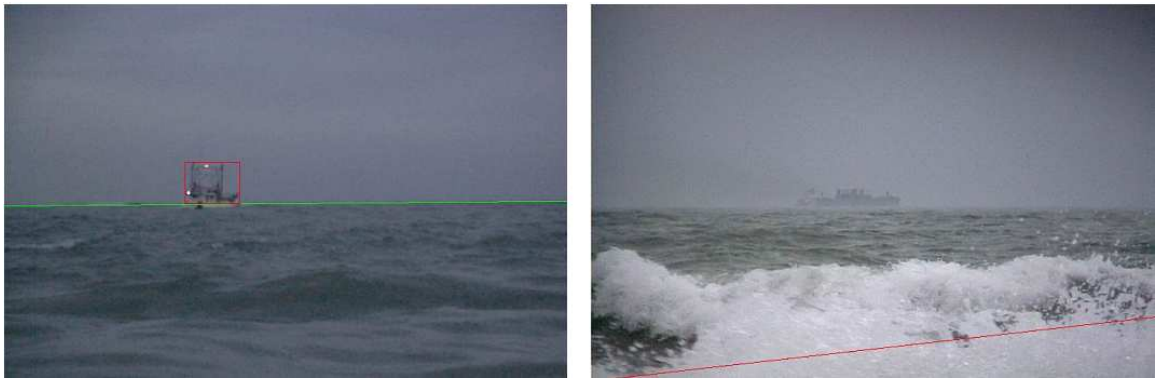

Figure 3.3. Horizon detection examples. Left images shows correct horizon identification, in the right image, because of the sea surf the horizon was detected incorrectly.

Figure 3.4. Examples of multiple detection of a single object.

a false positive and such results can be disregarded. The opposite situation may occur when a target in a frame is occluded by obstacles. For example a part of the ship may be occluded by water regions in the image or other ships in the ocean. In such a situation localization of the marine vehicle may not be possible because small objects are disregarded from consideration in the basic algorithm.

In order to tackle such problems video tracking of the detected targets is performed. To track the objects from frame to frame the idea of an observation and a state of an object is used. Observation and state of an object are time-related entities. The state of the objects reflects the true position of the objects in the environment at a particular time, or frame t. Observation shows the location of the target object detected by an algorithm. Having

several consecutive observations it is possible to decide the following about the state of the object: its location and behavior. It is also possible to predict the next state of the object based on a history of observations. Tracking of the object is considered successful when the prediction matches the actual measurement, i.e. when based on the history of observations of the object a prediction about the possible next location is made and confirmed by the real detection of the object in that location in the next frame. In relation to marine vehicle tracking it means, for example, that based on a 10 frame sequence the location of the marine vehicle is predicted for the 11th frame. If later, in the 11th frame, a detection algorithm shows the location of the marine vehicle that predicted location then the object is tracked successfully.

Tracking allows handling situations with false alarms and missed detections. If the history of object behavior does not support the measurement of its location, then such detection of an object in the current frame can be disregarded. This reduces the false alarm rate caused by the possible presence of noise in images. On the other hand, detection of an object can be considered for a certain location in a frame in the video even if the detection algorithm does not show presence of the object. That may happen when the history of the object from the previous and following frames shows consistent behavior.

The Kalman filter, described in Chapter 2, is a good framework to implement vision tracking of objects in video. The next subsection shows details of a filter implementation.

3.3.1 Use of the Kalman Filter

For this work two different filters are defined to track the following two entities: the position of the center of the bounding box (centroid) and the bounding box dimensions. Each of these two filters tracks the behavior of the two variables. Two auxiliary variables for each filter describe the speed of change the main variables. For example for the first filter the pair of variables that describe the position of the centroid - namely the x and y coordinates are supplemented by auxiliary variables that describe the speed of movement of this centroid along the x and y axes; horizontal and vertical dimensions of the bounding box

W and H are supplemented with the speed of changing of these variables in the horizontal and vertical directions.

Equations (3.1)–(3.2) show the implementation of the Kalman filter for visual tracking used in the thesis. The transformation matrix in (3.1) establishes the relation between the main and auxiliary variables in the current and next frames. That relation reflects the linear nature of the motion of the modeled object: the predicted value of the main variable (such as location of the corner) in the next state $k+1$ is different from the previous state k on the amount of value of the corresponding auxiliary variable Δx_k: $x_{k+1} = x_k + \Delta x_k$. The measurement matrix in (3.2) shows correspondence between the state vector and measurement vector. Other important variables used in the model are state w_k and measurement v_k noises which are described by a normal distribution.

$$\begin{bmatrix} x_{k+1} \\ y_{k+1} \\ \Delta x_{k+1} \\ \Delta y_{k+1} \end{bmatrix} = \begin{vmatrix} 1 & 0 & 1 & 0 \\ 0 & 1 & 0 & 1 \\ 0 & 0 & 1 & 0 \\ 0 & 0 & 0 & 1 \end{vmatrix} \begin{bmatrix} x_k \\ y_k \\ \Delta x_k \\ \Delta y_k \end{bmatrix} + w_k \tag{3.1}$$

$$\begin{bmatrix} x_{m_k} \\ y_{m_k} \end{bmatrix} = \begin{vmatrix} 1 & 0 & 0 & 0 \\ 0 & 1 & 0 & 0 \end{vmatrix} \begin{bmatrix} x_k \\ y_k \\ \Delta x_k \\ \Delta y_k \end{bmatrix} + v_k \tag{3.2}$$

Here x and y represent the main variables such as the position of the center or dimension of the bounding box. Δx and Δy are auxiliary variables.

The Kalman filter can tolerate big discrepancies, so called outliers in measurement or, as it is often called in computer vision, small occlusions. In the case that a tracking object is not found in a certain neighborhood of the predicted state it is considered that the object is hidden and will not use the measurement correction but instead only prediction.

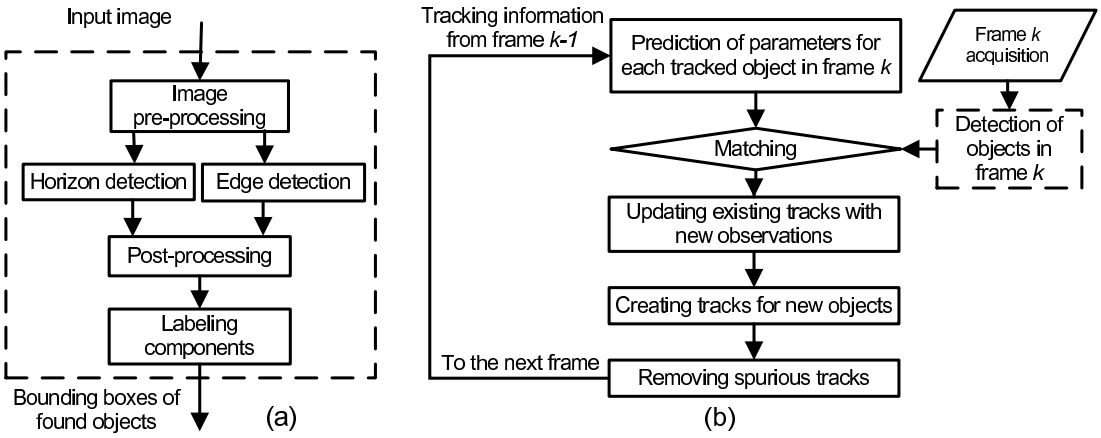

Figure 3.5. Outline of marine vehicle tracking algorithm. (a) Detection of marine vehicles in single image or frame. (b) Tracking of detected objects through video sequence.

3.3.2 Tracking of Marine Vehicles

Our algorithm for object tracking is similar to the Multiple Hypothesis Tracking (MHT) algorithm [38][39], but with significant modifications. The features of the algorithm include track initiation, continuation, and termination for multiple objects. Modifications introduced for the purpose of this work are related to the resolution of data association uncertainty as well as computational speedup.

Figure 3.5 shows the outline of the algorithm for tracking detected objects. The algorithm starts the iteration for the current frame by analyzing history of the previously tracked objects. It predicts the possible location and size of bounding boxes around objects by using a linear Kalman filter as described above. Independently the current frame is a subject of target detection by using the algorithm described in Section 3.2. Parameters of detected objects are compared with predictions. Those tracks that had their object found in the vicinity of the predicted location are updated to reflect the detection in the current frame. Tracks that did not receive evidence of the object in the current frame use the predictions instead of detections to avoid possible occlusions in the image. New tracks are initiated for objects that enter the frame or in the beginning of the video sequence. Tracks are terminated when objects leave the frame and also when tracks are not long enough. Objects are considered to be marine vehicles if they have substantial tracking history.

Association between the detected objects and tracks is considered a one-to-one mapping. The closest object in terms of euclidian distance is assigned to the track if it within the validation region for that track.

The track for a new object is initiated if the object that did not belong to any track was detected in two consecutive frames and the bounding boxes of such an object in these two frames intersect. Values for the state and measurement vectors for that track are initiated from these two frames. Such a simple initiation of a track creates many false alarms, but those false tracks are terminated quickly if the detection does not show consistency in the following frames. The track for an object is terminated if the number of valid detections in the history of the track is less than half of the number of consecutive frames for which the track exists. Objects with a track length of more that 20 frames are considered marine vehicles. Figure 3.6 shows 3-frame example from a video sequence with false alarms, true targets and their corresponding tracks.

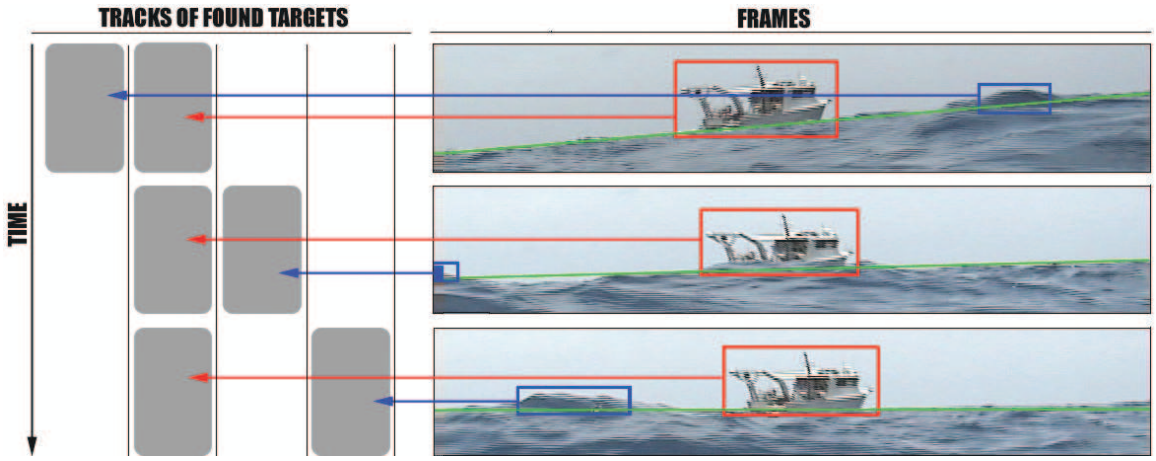

Figure 3.6. Example of tracking marine vehicles in video sequence. Sea waves are the main cause of false positives in basic detection algorithm. They are filtered out if the detections do not show consistency in between the frames.

CHAPTER 4

DATA AND PERFORMANCE EVALUATION

4.1 Overview

This chapter of the thesis describes quantitative measures to evaluate the results of marine vehicle detection and datasets used to evaluate the algorithms. One of the issues with the evaluation of ship detection performance in general is that it is often a subjective task: it is hard to say with 100% confidence if detection of an ship was carried out or not. Therefore methods for evaluation of performance are a very important part of any such system and should be defined in order to determine the success or failure of an algorithm, measure improvements, or produce a useful description of the results.

The accuracy of detection of marine vehicles in this thesis is measured by comparing output of the algorithm, or the candidate data, with the groundtruth, or target data. Groundtruth is a set of results which are created by a human. For this work groundtruth annotations were created by the researchers for both horizon and marine vehicles data in order to evaluation performance of algorithms for both categories.

Quantitative comparison for different detection algorithms is possible by using mechanism of metrics. Metrics provide a description of how well the candidate data matches the target data in a particular setting. Different metrics provide different aspects of performance of algorithms and each metric usually has its advantages and disadvantages. In content of this work metrics for both, horizon detection, and for the final result, marine vehicle detection, are defined for a single image and for a set of images.

4.2 Metrics for Horizon Detection Evaluation

The horizon is modeled as a single straight line with zero pixel thickness that separates two, assumably homogeneous, disjoint regions of pixels in the image - sky and ocean surface. Every line is characterized by its two parameters in polar coordinates: ρ distance to the origin of the coordinate system and Θ angle between the normal to the horizon line and the vertical axis (see Figure 4.1 (a)). Given such a representation of the horizon it is difficult to quantitatively compare lines in the target and candidate data just by the matching corresponding parameters. In order to answer the question of how close two description of horizon line are it was chosen to use pixelwise comparison of the candidate and target data. The groundtruth image for horizon detection consists of black and white pixels which are separated by envisioned horizon line. White pixels in such an image correspond to sky regions of the image and black pixels denote the ocean surface. Figure 4.1 (b) shows an example of such groundtruth.

Two metrics were chosen to reflect the accuracy of the horizon line detection. First accuracy performance metrics represents the percentage of pixels in the image (throughout the whole dataset) correctly separated into ocean surface and non-ocean surface regions by the found line:

$$A_1 = \frac{1}{k} \sum_{i=1}^{k} \frac{N_c^i}{N_i} \tag{4.1}$$

where k is the number of images in the dataset, N_c^i - number of pixels correctly separated by the found horizon line in image i, N_i - number of pixels in the image i. This metric provides a reference to a general performance of an algorithm on a dataset of images. Its main disadvantage is that bad visual performance of horizon detection on some images may stay unnoticed by the such metric output if the majority of other images in the dataset are processed well.

Second metrics is aimed to reflect performance of the algorithm on each of the image of the dataset. The horizon line in an image is considered to be detected correctly if the

Figure 4.1. Horizon representation. (a) The horizon is represented as a straight line in polar coordinates with parameters ρ and Θ. (b) Groundtruth for an image. The white color regions corresponds to the sky (above the horizon), black regions correspond to the ocean surface.

percentage of pixels in the image correctly separated by the horizon line is above a specified threshold. The percentage of such images in the dataset will define the second accuracy metric:

$$A_2 = \frac{n_c}{k} \tag{4.2}$$

where k is the total number of images in the dataset and n_c is the number of images in the dataset where the horizon line was detected with accuracy above the given threshold:

$$\frac{N_c^i}{N_i} \geq T \tag{4.3}$$

where T is the threshold value.

Another important characteristic for which the horizon detection algorithms were evaluated was the running time of the algorithms. The main requirement for fast performance may come from systems that do real time processing of video data or systems where the number of CPU cycles used for detection is required to be at the minimal level in order satisfy power consumption constraints.

4.3 Metrics for Marine Vehicle Detection Evaluation

Detection of marine vehicles is more complicated than horizon detection and thus, more aspects need to be evaluated. In single images detection implies spatial localization of found ships (allowing multiple vessels per image). In video, combination of spatial and temporal dimensions requires tracking the target from frame to frame, thus temporal localization of the same objects throughout the frame sequence should be performed.

Marine vehicles considered for detection in images and video are, in most cases, compact objects and therefore can be covered by simple bounding shapes. It was chosen to use rectangular bounding box as a shape to mark the groundtruth and output data of the algorithm. For simplicity of representation, the bounding box is always oriented so that its sides are parallel to the axes of the image plane. Each groundtruth image is a binary image where white regions correspond to background and black rectangular regions correspond to the target objects.

Process of creating groundtruth for marine vehicles is tedious when the number of groundtruth images is substantial. To facilitate creation of groundtruth the author used software ViPER [40] to create bounding boxes around targets in the data. ViPER tool was created to provide repeatability and comparability in performance evaluation. Attributes of descriptors, such as bounding boxes, may be recorded for arbitrary sets of consecutive frames in the video which makes such tool very convenient for the researcher.

Detection and tracking measures for performance evaluation were adopted from [41]. These comprehensive metrics account for important measures of system performance such as number of objects detected and tracked missed objects, false positives, fragmentation in both spatial and temporal dimensions, and localization error of detected objects. The following notations are used to define the metrics:

- G_i denotes i^{th} target object at the sequence level and $G_i^{(t)}$ denotes the i^{th} target object in frame t.
- D_i denotes i^{th} candidate object at the sequence level and $D_i^{(t)}$ denotes the i^{th} detected object in frame t.

- $G^{(t)}$ is the set of targets in a single image t
- $D^{(t)}$ is the set of candidates from the algorithm.
- N_G and N_D denote the number of unique targets and number of unique candidates for the sequence of frames.
- N_{frames} denotes the number of frames in the sequence.
- N_{mapped} is the number of mapped target and candidate pairs.

Frame Detection Accuracy (FDA) is the metric that reflects accuracy of detection localization. It calculates the overlap between the target and candidate objects as a ratio of the spatial intersection between the two objects and the spatial union of them. The sum of all of the overlaps is normalized over the average of the number of targets and candidates. For a frame t with $N_G^{(t)}$ targets and $N_D^{(t)}$ candidates $FDA(t)$ is defined as follows:

$$FDA(t) = \frac{OverlapRatio}{[\frac{N_G^{(t)} + N_D^{(t)}}{2}]} \tag{4.4}$$

$$where, \quad OverlapRatio = \sum_{i=1}^{N_{mapped}^{(t)}} \frac{|G_i^{(t)} \bigcap D_i^{(t)}|}{|G_i^{(t)} \bigcup D_i^{(t)}|} \tag{4.5}$$

Sequence Frame Detection Accuracy metric shows the performance of detection for the whole frame sequence. This metrics accounts for both missed detects and false positives in one score. It is expressed as FDA calculated over all of the frames in sequence and normalized to the number of frames in the sequence where targets or candidates existed:

$$SFDA = \frac{\sum_{t=1}^{t=N_{frames}} FDA(t)}{\sum_{t=1}^{t=N_{frames}} \exists(N_G^{(t)} OR \ N_D^{(t)})} \tag{4.6}$$

Next metrics are similar to the horizon metric (4.2). They take hard decision for each target object: detected or not detected. A target object is considered detected if minimum proportion of its area is covered by the candidate. Thresholded Overlap Ratio

and Thresholded Frame Detection Accuracy (FDA-T) are defined as follows:

$$ThresholdedOverlapRatio = \frac{FDA - T}{|G_i^{(t)} \bigcup D_i^{(t)}|} \tag{4.7}$$

where

$$FDA - T = \begin{cases} |G_i^{(t)} \bigcup D_i^{(t)}|, & if \quad \frac{|G_i^{(t)} \bigcap D_i^{(t)}|}{|G_i^{(t)} \bigcup D_i^{(t)}|} \geq Threshold \\ |G_i^{(t)} \bigcap D_i^{(t)}|, & if \quad \frac{|G_i^{(t)} \bigcap D_i^{(t)}|}{|G_i^{(t)} \bigcup D_i^{(t)}|} < Threshold \ \& \ non - binary \ thresholding \\ 0, & if \quad \frac{|G_i^{(t)} \bigcap D_i^{(t)}|}{|G_i^{(t)} \bigcup D_i^{(t)}|} < Threshold \ \& \ binarythresholding \end{cases} \tag{4.8}$$

The Sequence Track Detection Accuracy (STDA) is a measure of tracking performance over all of the objects in the sequence and is calculated as following:

$$STDA = \sum_{i=1}^{N_{mapped}} \frac{\sum_{t=1}^{N_{frames}} [\frac{|G_i^{(t)} \bigcap D_i^{(t)}|}{|G_i^{(t)} \bigcup D_i^{(t)}|}]}{N_{(G_i \bigcup D_i \neq 0)}} \tag{4.9}$$

The Average Tracking Accuracy (ATA) is defined as STDA per objects:

$$ATA = \frac{STDA}{[\frac{N_G + N_D}{2}]} \tag{4.10}$$

ATA is a spatio-temporal metric which penalizes fragmentations in the temporal and spatial dimensions. It accounts for the number of objects detected and tracked, missed objects, and false positives.

4.4 Datasets

The datasets discussed in this work were used to evaluate performance of detection of two categories of entities: marine vehicles and the horizon. The final result of the work is evaluation of detection of marine vehicles in single images and in video. The need to evaluate horizon detection algorithms was due to high correlation between correct horizon detection and good accuracy in detecting marine vehicles. Chapter 5 compares different

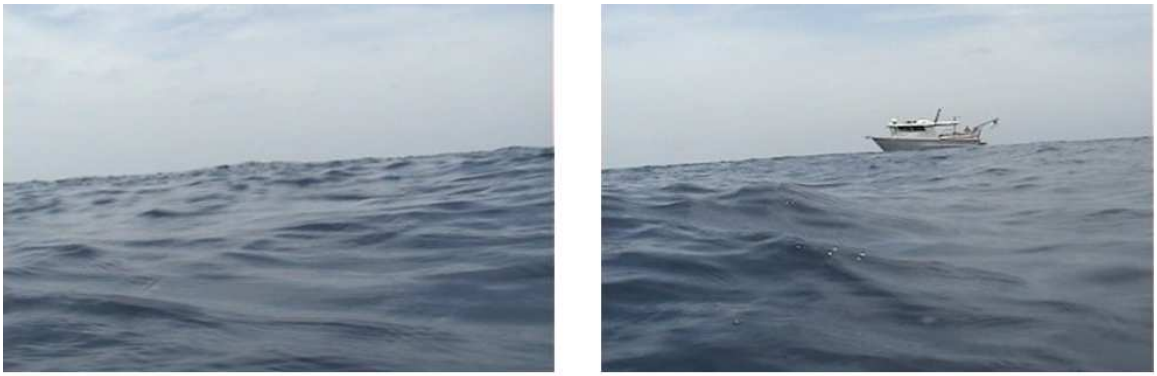

(a) (b)

Figure 4.2. Examples of images from datasets used for testing horizon detection algorithms. (a) HORIZON DATASET 1 - no floating objects, clear horizon; (b) HORIZON DATASET 2 - marine vehicles presents on the horizon line. Data of the same nature was used in SHIP DATASET 2

horizon detection algorithms in terms of accuracy of horizon detection on the two datasets of images.

The first dataset, further referred as HORIZON DATASET 1, was chosen to test the general characteristics of the horizon detection algorithm: ability to correctly detect horizon line in images where only sea and sky region were present. This dataset consisted of 160 frames chosen randomly from video sequences taken by a camera installed on a buoy in the open sea. A separate set of 10 similar frames was used for training purposes. All images (frames of the video) were color images of resolution of 720x480.

The second dataset, referred to as the HORIZON DATASET 2, represented 150 frames picked in a similar way from video sequences taken by the same buoy camera. Many of these images contained ships, floating objects, or waves that made the horizon line look uneven. Examples of images in both horizon datasets are shown in Figure 4.2.

Groundtruth for both sets was created as described in Section 4.2. For images where the waves, ships, or other objects were present this groundtruth line represented the horizon envisioned without any objects. This location of horizon line would provide the best cue for further segmentation of the image in order to locate the sought marine vehicles.

For evaluation of performance of the marine vehicles detection algorithm datasets of still images and video sequences were used. Hereafter, SHIP DATASET 1 refers to the

dataset of 100 images taken by a digital camera in daylight conditions. The camera was installed onshore and the images contained only ocean surface, floating objects including ships. The images did not contain any coastal objects. All images in the dataset were in resolution of 1280x960. Figure 4.3 shows a sample image from this dataset.

The second dataset for marine vehicle evaluation, further referred to as SHIP DATASET 2, consisted of 30 video sequences. The video for the dataset was taken from a digital camcorder mounted on a buoy in open ocean in daylight. The content of the video is the ocean surface with possible single ship present and no coastal objects. The mentioned marine vehicle in the video sequence could be present the whole time, could enter or leave the frame at some point of time, or be absent throughout the video sequence. Each video sequence was 10 seconds long and contained 300 frames (30fps) and was created at a resolution of 720x480. The total number of frames in the dataset is 9000. Original video sequences from the camcorder were recorded in MPEG-1 format but the data for the algorithm were fed frame by frame. An important aspect of the SHIP DATASET 2 is the fact that, although, the nature of the data is sequential, the algorithms were tested to detect marine vehicles in both settings. In the first setting the frames of the videos were considered independently from neighboring frames to test detection of the basic algorithm as in single images. In the second setting considered tracking a marine vehicle from frame to frame and, thus, was working on these frames as with ordered sequence.

Images for horizon detection datasets were of the same nature as SHIP DATASET 2, so Figure 4.2 can serve for illustration purposes of data in SHIP DATASET 2 as well. Groundtruth for the both ship datasets was created as described in Section 4.3. Chapter 6 discusses results for detection of marine vehicles.

Figure 4.3. Example image from SHIP DATASET 1 used for testing marine vehicles detection algorithm.

CHAPTER 5

COMPARISON OF HORIZON DETECTION ALGORITHMS

5.1 Overview

Detection a ship in the vicinity of the horizon line is much easier and reliable than trying to segment out a ship-blob out of the whole horizon image. Horizon detection is more robust and its precise identification reduces the possible search space for marine vehicles. Also segmentation of a ship out of the sky background can be performed with simple image processing techniques compared to complex methods of object segmentation out of the whole sky-sea image.

This chapter investigates the performance of the horizon detection algorithms described in Chapter 1 on two different datasets of horizon images (see Section 4.4). The first set, HORIZON DATASET 1, contains only horizon images of clear ocean surface without marine vehicles (see Figure 4.2 (a)). The second test set, HORIZON DATASET 2, introduces ships and other floating objects on the horizon which generally influence horizon detection (See Figure 4.2 (b). Some modifications to the original algorithms, introduced for the purpose of better performance of "ship images" were tested on the second dataset.

Particular re-implementations of horizon detection algorithms and their modification will be named.

The horizon detection algorithms described in Chapter 1 were developed by teams of researchers mostly for projects related to navigation of unmanned aerial vehicles (UAV). Requirements for these algorithms were quite different from the requirements for the algorithm described in this work. While navigation of UAV needs the horizon line in order to avoid obstacles that are assumed to be below the horizon our application needs the horizon line for reliable marine vehicle segmentation in images and video sequences which are as-

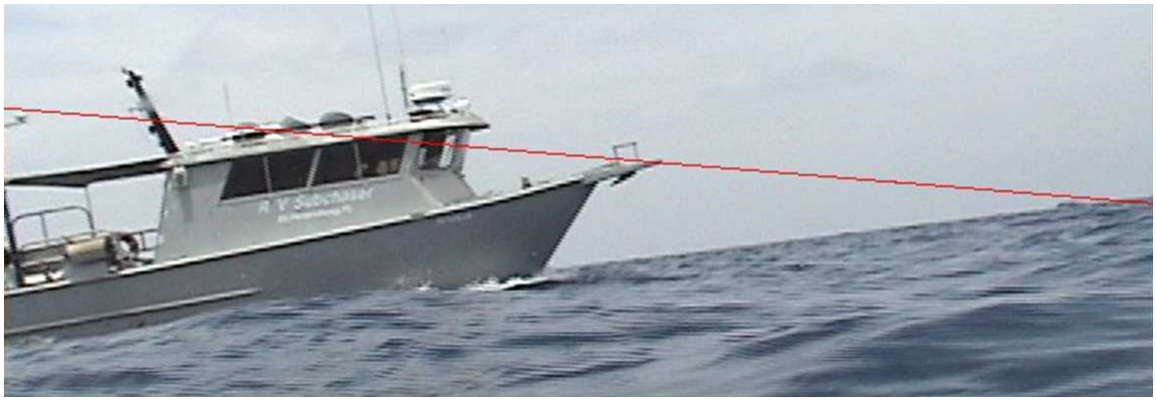

Figure 5.1. Example of failure of horizon detection. Assumption that the image consists of two regions - sky and non-sky leads to the detection of horizon line above the vessel.

sumed to be located above the envisioned horizon line. Output of the algorithms that may be suitable for navigation of UAV may not be appropriate for detection of marine vehicles. Figure 5.1 shows the result of the horizon detection algorithm described in [18]. Because of the vessel present in the image the algorithm found the line that best separates sky and non-sky image lies above the sought ship, a result not acceptable for our application.

The literature review section of this document contains references to five categories of approaches to detect horizon in images. Some of these approaches [26, 27] rely on specific hardware to obtain images, and, thus, are not appropriate in the context of our algorithm. The approach described in [21, 22] was designed to use the horizon as an estimator for roll and pitch angle, and precision of the horizon line in the image itself was not the primary target. The angle of the horizon is determined by taking the perpendicular of the line joining sky and non-sky centroids. In case of rectangular images (source of our data), the line between the centroids does not turn out exactly perpendicular to the horizon. In addition the process of assigning labels to pixels into sky/non-sky classes based just on the grayscale intensity value is in itself very inaccurate. An interesting and fast approach [23] to apply a projection profile to an edge-image is good enough for straight horizon lines with little texture (source of edges) coming from the ocean surface. But as it was tested with some images from our evaluation dataset this may not be the case, and some anomalies in horizon detection are observed even for simple images.

It was decided to concentrate on two main categories of approaches for horizon detection. The first category, described in a number of papers [17, 18, 19, 20], is a statistical approach that tries to minimize intra-class variance between two categories of pixels. This approach does not assume any training and is referred to as unsupervised. The second category of algorithms, described in [24, 25], assumes training of a classifier on some labeled data and is referred as supervised approach. The next two sections describe in detail these original algorithms. The following sections show some modifications to these algorithms during our re-implementation, as well as a comparison of performance of these algorithms.

5.2 Horizon Detection: Unsupervised Approach

The unsupervised approach [18] to horizon detection algorithm uses two basic assumptions:

- the horizon line appears in the image approximately as a straight line; and
- the horizon line separates the image into two regions that have different appearance - sky and non-sky. In the sky region pixels will look more like other sky pixels, and less like non-sky, and vice versa.

The first assumption reduces the search space for all possible horizons to a two-dimensional search in line-parameter space. For each possible line in that two-dimensional space a special criterion determines how well that particular line agrees with the second assumption or in other words how well the correct horizon line separates the image into two regions that have different appearance. The method utilizes the normal representation of a line (see Figure 4.1 (a) for illustration):

$$x \cos \Theta + y \sin \Theta = \rho \tag{5.1}$$

where (x, y) are the coordinates of the points on the line, Θ is the angle representing the rotation of the line, and ρ is the perpendicular distance from the line to the origin.

The RGB color was chosen as a measure of appearance. For any given hypothesized horizon line, the pixels above the line are labeled as sky, and pixels below the line are labeled as non-sky. All hypothesized sky pixels are denoted as,

$$x_i{}^s = [r_i{}^s g_i{}^s b_i{}^s], \qquad i \in \{1, \ldots, n^s\} \tag{5.2}$$

where $r_i{}^s$ denotes the value for intensity of the red channel in RGB, $g_i{}^s$ denotes the green channel value and $b_i{}^s$ denotes the blue channel value of the i-th sky pixel. All the hypothesized non-sky pixels are noted as,

$$x_i{}^g = [r_i{}^g, g_i{}^g, b_i{}^g], \qquad i \in \{1, \ldots, n^s\} \tag{5.3}$$

Given these pixel groupings, the assumption that sky pixels look similar to other sky pixels, and that non-sky pixels look similar to other non-sky pixels is quantified. One measure of this is the degree of variance exhibited by each distribution. The proposed optimization criterion for such variance is the following:

$$J(\Theta, \rho) = \frac{1}{\Sigma_s + \Sigma_g} \tag{5.4}$$

based on the covariance matrices and of the two pixel distributions,

$$\Sigma_s = \frac{1}{n_s - 1} \sum_{i=1}^{n_s} (x_i{}^s - \mu_s)(x_i{}^s - \mu_s)^T \tag{5.5}$$

$$\Sigma_g = \frac{1}{n_g - 1} \sum_{i=1}^{n_g} (x_i{}^g - \mu_g)(x_i{}^g - \mu_g)^T \tag{5.6}$$

where n_s is the number of sky-pixels, n_g - number of non-sky pixels, and μ_s and μ_g are mean vectors for color-intensity of the sky and non-sky pixel distributions and are defined as

$$\mu_s = \frac{1}{n_s} \sum_{i=1}^{n_s} x_i^s, \quad \mu_g = \frac{1}{n_g} \sum_{i=1}^{n_g} x_i^g \tag{5.7}$$

Assuming that the means of the actual sky and ground distributions are distinct, the line that best separates the two regions should exhibit the lowest variance from the mean. If the hypothesized horizon line is incorrect, some non-sky pixels will be mistakenly grouped with sky pixels and vice versa. The incorrectly grouped pixels will lie farther from each mean, consequently increasing the variance of the two distributions. The incorrectly grouped pixels will skew each mean vector slightly, contributing further to increased variance in the distributions.

5.3 Horizon Detection: Supervised Approach

The approaches described in [24] and [25] use machine learning techniques to classify each pixel in the image into sky and non-sky class based on its color and texture of a region around it. The classification of the image into sky and non-sky in [24] is performed using a support vector machine (SVM) classifier [42] that assigns a category for each pixel based on its color in the RGB color space, after smoothing the image with a Gaussian filter to reduce the effects of noise. The approach described in [25] compares multiple classifiers and uses multiple texture features along with the color of pixels. The authors of the paper conclude that SVM performs better than other classifiers due to the fact that SVM is inherently a binary classifier.

Although idea of pixel classification is similar in both approaches methods of finding the actual horizon line from the classified image are different. In [24] the horizon is found by searching for the line that best represents the boundary between binary sky segmented image into sky and ground. The first step is to apply standard morphology operations of erosion and dilation [28], [32] to the binary segmented image to remove any small sections of misclassified pixels. The border between sky and ground regions is then found by smoothing the binary image and classifying all pixels with values near 0.5 as boundary pixels. The horizon line detection is performed using the Hough transform [28] on the border image with a normal representation of a line. Each line in (X, Y) space can be represented by a point in (Θ, ρ) space. Conversely, each point in the (X, Y) space represents a set of lines

in (Θ, ρ) space, which correspond to all of the possible lines that pass through that point. Thus, for each point in (X, Y) space, a vote is placed in each bin of a discretized (Θ, ρ) space that corresponds to all possible lines that pass through that point. Bins in (Θ, ρ) space that receive a large number of votes correspond to probable lines. The best horizon is chosen as the candidate line which minimizes the cost function:

$$J(\Theta, \rho) = \sum_{i,j} \vec{e}(\vec{x}_{ij}) \tag{5.8}$$

$$\vec{e}(\vec{x}_{ij}) = \begin{cases} 0 & \text{if } f(\vec{x}_{ij}) = 1, \quad (i,j) \text{ is above horizon} \\ \alpha & \text{if } f(\vec{x}_{ij}) = -1, \quad (i,j) \text{ is above horizon} \\ 1 & \text{if } f(\vec{x}_{ij}) = 1, \quad (i,j) \text{ is below horizon} \\ 0 & \text{if } f(\vec{x}_{ij}) = -1, \quad (i,j) \text{ is below horizon} \end{cases} \tag{5.9}$$

where f(x) is the classification output, 1 for sky, -1 for ground, x_{ij} is the color vector from the pixel at (i, j) in the image, and α is a positive constant. Thus, $J(\Theta, \rho)$ is a weighted sum of all of the pixels above the candidate horizon classified as non-sky and all of the pixels below the candidate horizon classified as sky.

The other method [25] in order to find horizon line in a classified image uses an approach similar to the one described in Section 5.2. But instead of color information used to describe each pixel, binary information (class of a pixel) is used.

5.4 Horizon Detection Performance on the Dataset without Ships

The algorithms that were tested on this dataset of images included the horizon detection algorithm described in Section 5.2, a derivation of it that includes texture, and an algorithm [24] described in Section 5.3. The algorithm [25] which uses classification of pixels in the image into sea surface/non-sea surface based on many texture features was not considered

because of many computationally-intensive texture measurements needed to be performed, operations that make the run-time prohibitively big.

The algorithm from [18], further called UNSUPERVISED, was implemented based on the paper's description as the search for the best parameters in two steps. During the first step the algorithm used the image scaled to 1/5 of the original dimension in order to find approximate parameters' values. Scaling of the image is done for the purpose of speeding up the computations. The second step searches for the horizon parameters in the original image (without scaling) but uses the result of the first step as a starting point and the search is performed in the limited vicinity of the search result of the first step, thus, refining the result of the first step. Features used to distinguish sky and non-sky regions are RGB intensity of the pixels that comprise them available directly from the input image.

A derivation of the UNSUPERVISED algorithm that uses texture information, further called UNSUPERVISED-TEXTURE, uses the same two-step approach to find the horizon parameters, but along with RGB colors it also incorporated texture measurement of uniformity (see (2.11) and Figure 2.2 (g) for illustration). Uniformity was chosen out of the number of texture features described in Section 2.4 because it provides more distinction for values in sea surface/non-sea surface regions. This texture measurement was assigned to each pixel in the image and was calculated as a measurement of uniformity in the grayscale patch of 10x10 pixels around the target pixels.

The last algorithm considered for evaluation [24], described in Section 5.3, is based on classification of pixels into sea surface/non-sea surface. Further in the text this algorithm is referred as SUPERVISED algorithm. To train the classifier 10 images of the training set were used. The total of 1% pixels in each out of 10 training images was chosen randomly to create a set of training vectors (about 38,000 vectors). The classification results were followed by morphology operations of erosion and dilation with a structural element of disk with radius equal to 7 pixels.

The Table 5.1 shows the performance results for the three algorithms obtained on the HORIZON DATASET 1 with the metric described by (4.1). The results are shown for the

accuracy range of 82% and above, where the described horizon detection algorithm show the biggest difference in performance.

Table 5.1. Accuracy of the horizon detection algorithms on the HORIZON DATASET 1 according to metric (4.1).

	UNSUPERVISED	SUPERVISED	UNSUPERVISED TEXTURE
Accuracy of Detection According to (4.1)	99.26%	98.89%	97.94%

Table 5.2 shows the performance of the same algorithms using the second metrics described by (4.2). The chart in Figure 5.2 shows the same results visually.

Table 5.2. Accuracy of the horizon detection algorithms on the HORIZON DATASET 1 according to metric (4.2).

	THRESHOLD									
Algorithm	84%	86%	88%	90%	92%	94%	96%	97%	98%	99%
UNSUPERVISED	98.75%	98.75%	98.75%	98.75%	98.75%	98.75%	98.75%	98.75%	97.50%	95.00%
SUPERVISED	98.75%	98.75%	98.12%	98.12%	96.88%	95.63%	95.00%	94.37%	92.50%	91.25%
UNSUPERVISED TEXTURE	99.38%	99.38%	98.75%	97.50%	96.88%	93.13%	86.25%	76.88%	65.63%	46.88%

Table 5.3 shows running time in seconds per image for these algorithms. The algorithms were implemented in MATLAB environment and tested on AMD Athlon 64 X2 Dual 3 GHz processor. For the SUPERVISED algorithm the running time does not include training time. Training of the algorithm is supposed to be done offline.

Table 5.3. Running time of the horizon detection algorithms on HORIZON DATASET 1 in relative time units per image.

	UNSUPERVISED	SUPERVISED	UNSUPERVISED TEXTURE
Running time (time units)	17.1	1.4	44.4

The result of comparison excludes the UNSUPERVISED TEXTURE algorithm from further consideration because of its inferior accuracy and significant running time.

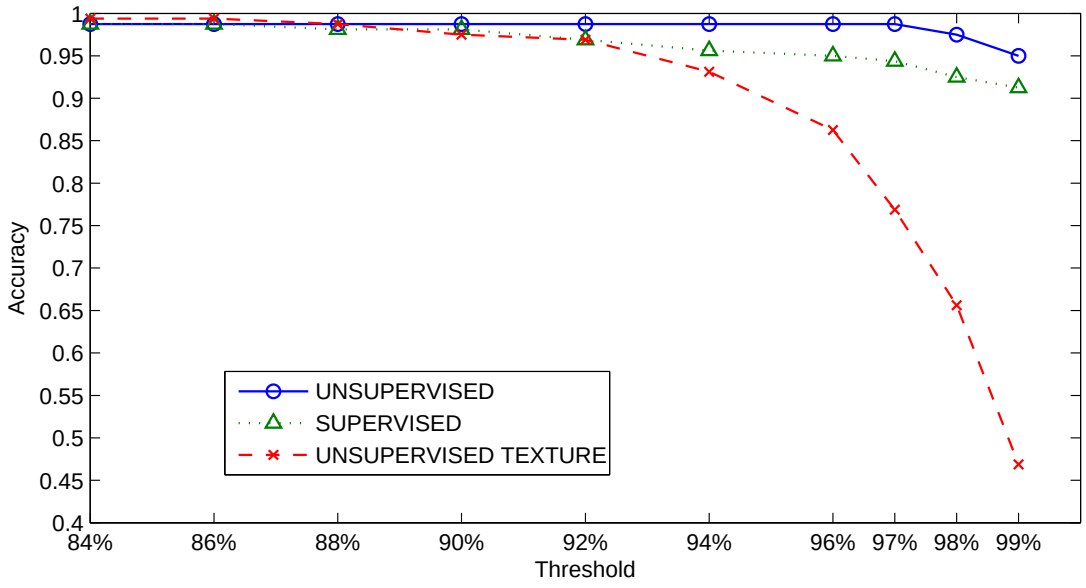

Figure 5.2. Accuracy of horizon detection algorithms on HORIZON DATASET 1, metric (4.2) is used.

5.5 Horizon Detection Performance on the Dataset of Images with Floating Objects Present

The algorithms tested in this experiment included UNSUPERVISED, SUPERVISED algorithms, and another derivative of UNSUPERVISED algorithm. As mentioned before one of the problems with horizon detection algorithms, especially with UNSUPERVISED, is that the optimal line for horizon may be skewed by possible objects present on the horizon line. A marine vehicle may be one of these objects.

A derivative of the UNSUPERVISED algorithm, further referred as UNSUPERVISED SLICE, applies the same idea for horizon detection as the original UNSUPERVISED algorithm: the sought horizon line is the line that best separates homogeneously colored two distributions, sea surface/non-sea surface. The algorithm divided the original image into n disjoint vertical slices (in this particular implementation n was chosen to be 20) and finds horizon line in each of these. The horizon line for the whole image is found as the combination of the "small horizons" in these slices of the original image. The idea behind this technique is to disregard those slices where the floating objects skew the result for the

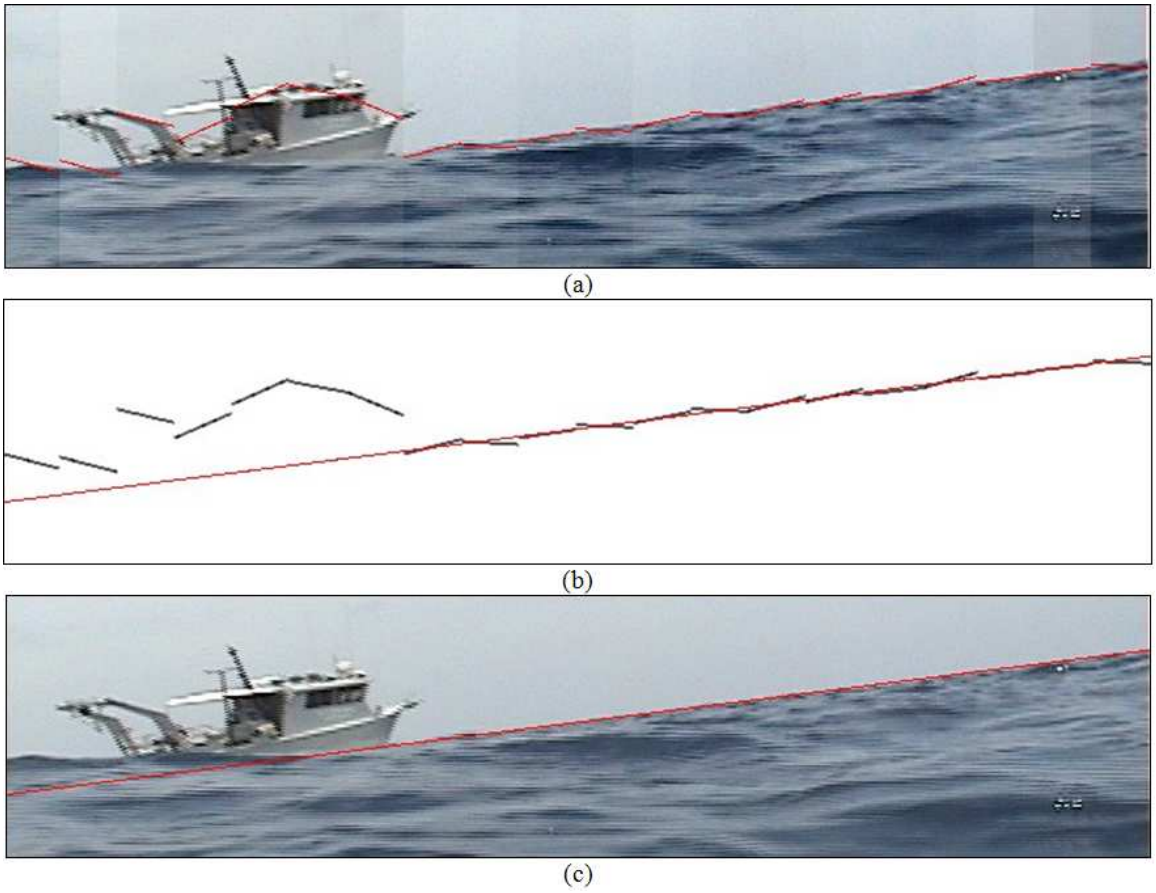

Figure 5.3. Steps of UNSUPERVISED-SLICE algorithm. (a) horizon lines are found for each of the slices in the original image. (b) Hough transform applied on synthesized image containing only horizon lines for the slices. Red line shows the horizon found. (c) Found horizon superimposed on the original image.

whole image. Possible techniques for such combination of "small horizons" may include the median filter, where only a part of the values for horizon is used, the Hough transform for image of combined horizons, or a technique similar to weighted-majority algorithm [43]. UNSUPERVISED SLICE algorithm evaluated in this experiment used Hough transform. It was applied to a binary image of combined horizon results from slices of the original image. Figure 5.3 shows steps of the UNSUPERVISED SLICE algorithm as an example. It shows that the horizon lines found for slices, where the ship was observed, have been disregarded and did not contribute towards the final horizon line.

Table 5.4. Accuracy of the horizon detection algorithms on HORIZON DATASET 2 according to metric (4.1).

	UNSUPERVISED	SUPERVISED	UNSUPERVISED SLICE
Accuracy of Detection According to (4.1)	98.41%	99.29%	99.41%

Table 5.5. Accuracy of the horizon detection algorithms on HORIZON DATASET 2 according to metric (4.2).

	THRESHOLD									
Algorithm	84%	86%	88%	90%	92%	94%	96%	97%	98%	99%
UNSUPERVISED	96.67%	95.33%	94.67%	94.67%	94.67%	94.67%	92.00%	92.00%	88.00%	82.67%
SUPERVISED	100%	100%	100%	100%	100%	100%	100%	100%	100%	100%
UNSUPERVISED SLICE	100%	100%	100%	100%	100%	100%	100%	98.67%	95.33%	88.00%

The performance of the three algorithms on the HORIZON DATASET 2 for both metrics of accuracy and running time is shown in Tables 5.4, 5.5, 5.6 and Figure 5.4.

Table 5.6. Running time of the horizon detection algorithms on HORIZON DATASET 2 in relative time units per image.

	UNSUPERVISED	SUPERVISED	UNSUPERVISED SLICE
Running time (time units)	17.1	1.4	25.1

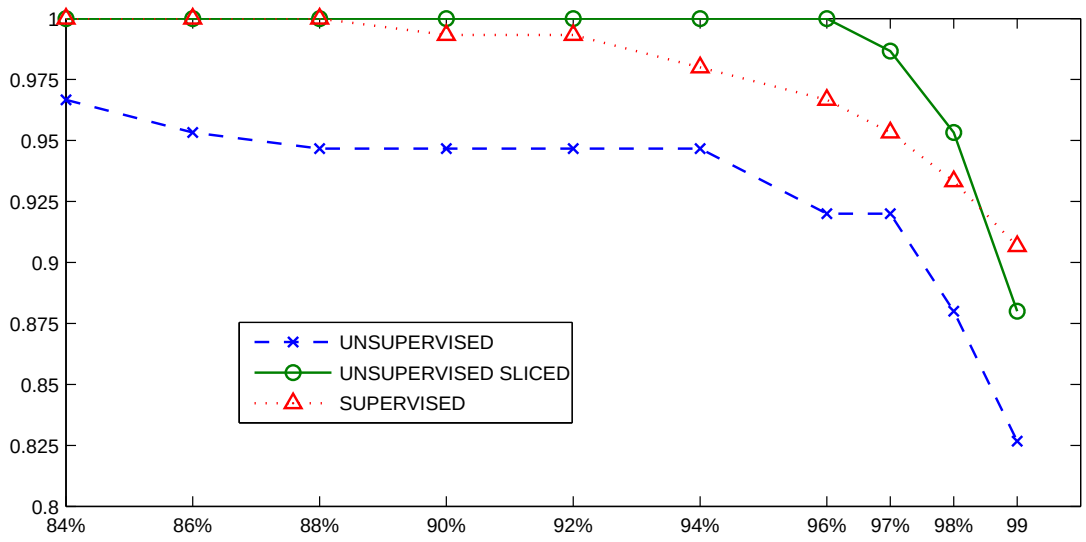

Figure 5.4. Accuracy of horizon detection algorithms on HORIZON DATASET 2, metric (4.2) is used.

5.6 Selection of Horizon Detection Algorithm

The horizon detection algorithms evaluated in this chapter are important for accurate ship segmentation. For our application performance of the algorithms on the HORIZON DATASET 2 is more of consideration because the realistic data for a future application may include floating objects. Two algorithms performed well on that dataset - the UNSUPERVISED SLICE and SUPERVISED. The UNSUPERVISED SLICE is the horizon detection algorithm of our choice in the overall detection scheme.

It is worth mentioning that while the UNSUPERVISED SLICE is better in terms of accuracy, it has a notable disadvantage. The UNSUPERVISED algorithm and its derivatives work as unsupervised-classifiers which always try to draw a line between the two most distinct regions in the image, i.e. two clusters: sea surface and non-sea surface. For some situations when an image may contain only sky or only sea surface pixels, or different regions of the sea surface have more distinction then major categories of sea and sky such clasterization may lead to poor performance results. The SUPERVISED algorithm is more adjustable for such situation because its classifier can be trained (however, the performance may suffer if the training data is limited). In addition classification of pixels and subsequent Hough transform is done much faster compared to the search in parameter space performed by the UNSUPERVISED algorithm and its derivatives. With future modifications and heuristics a derivative of the SUPERVISED algorithm may match The UNSUPERVISED SLICE in terms of performance.

CHAPTER 6

RESULTS ON MARINE VEHICLE DETECTION

This chapter of the thesis evaluates the final results of ship detection using the algorithm described in previous chapters. The image and video datasets as well as performance metrics described in Chapter 4 were used to evaluate the proposed ship detection technique. The UNSUPERVISED SLICE horizon detection algorithm, described in Chapter 5, was used to detect the horizon line.

6.1 Performance of Algorithm on Single Images

During this experiment each image in SHIP DATASET 1 was processed separately. No tracking was possible and thus only a basic detection scheme described in Section 3.2 and shown in Figure 3.1 was used. The following parameters(found empirically) and settings were used:

- The shape of a structural element for morphology operations used is disk.
- The size of the structural element for initial erosion is 2 pixels.
- The size of the structural element for the following dilation is 7 pixels.
- Minimum size of a marine vessel in any dimension should be 6 pixels.
- A found objects should be within 10 pixels from the horizon line in order to be considered a ship.

Table 6.1 shows the performance of the algorithm on SHIP DATASET 1 recorded using Sequence Frame Detection Accuracy metric for binary and non-binary threshold options (SFDA BT, SFDA NBT). The regular SFDA metric shows 75% accuracy value. There

were no missed objects. The rate of false alarms was 3%. Figure 6.1 shows examples of the detection of ships in single images from a forward-looking camera.

Figure 6.2 shows typical failures in detection localization on SHIP DATASET 1. Most of the time false alarms point out part of the real targets, which have already been detected (fragmentation problem).

Table 6.1. Result of marine vessel detection in single images.

Threshold Value	SFDA NBT	SFDA BT
0.2	94.02%	88.80%
0.4	86.96%	75.87%
0.6	53.26%	41.57%
0.8	27.17%	15.88%

6.2 Performance of Algorithm on Video Sequences

The performance of the ship detection algorithm on video was evaluated on the SHIP DATASET 2 which was described in Section 4.4. The experiment was conducted with the same settings and parameters for the basic detection part as for the experiment with single images. The parameters and settings used for the tracking part of the algorithm include the following:

- A track is initiated if the object is present in two frames and its bounding boxes in two frames spatially intersect.
- The parameters of the Kalman filter for the track are initialized from these two frames
- The valid variation of location and size of the bounding box is obtained from covariance matrix for the state vector. The detection of the object in a frame is confirmed if it is within the validation range for it's location and size predicted from the previous measurement.
- If the object has not been detected in a frame the prediction is used as the actual measurement in order to continue tracking.

Table 6.2. SFDA metrics for two different settings: on individual frames and on video sequence with tracking.

	Individual Frames Without Tracking			Video Sequences With Tracking		
Threshold	SFDA	SFDA NBT	SFDA BT	SFDA	SFDA NBT	SFDA BT
0.2	33.18%	53.68%	52.17%	68.85%	92.43%	92.29%
0.4		45.26%	38.72%		88.65%	80.18%
0.6		34.92%	28.67%		83.42%	67.07%
0.8		26.88%	19.22%		72.64%	48.16%

- A track is terminated if the number of valid detections in a track sequence is less than half of the length of the track sequence.

- The object is considered a marine vehicle and is shown in algorithm's output if the track has a length of no less than 20 frames. This parameter was chosen manually in order to avoid detection of sea waves. For different frame-per-second setting of the video sequence this parameters should be changed.

The Sequence Frame Detection Accuracy (SFDA), Sequence Frame Detection Accuracy Non-Binary Threshold (SFDA NBT), and Sequence Frame Detection Accuracy Binary Threshold (SFDA BT) metrics were calculated on the dataset of video sequences for two settings: for the results of detection for marine vehicles independently in each frame and for the results of marine vehicles detected and tracked in video sequences. Such a setup of the experiment allows evaluation of improvement which gives the addition of the tracking algorithm to the basic detection algorithm. The miss rate and false alarm rate were calculated for the second setting.

Table 6.2 shows the performance according to those metrics. The value for each setting reflects SFDA performance averaged from all 30 video sequences present in the dataset. SFDA-threshold settings show the performance of the algorithm according to four threshold values chosen to reflect the spatial localization aspect of the algorithm. Results for the setting where detected objects were tracked through the video sequences show significant improvement over independent detection in single frames. The reason for improvement is in substantial reduction of false alarms. Overall, the visual results of detection are promising: targets were detected and tracked in all video sequences of the dataset. Missed objects at

the 2.27% rate. The rate of false alarms was 11%. Figure 6.3 shows examples of detection of ships in video.

It is worth mentioning that the performance of the algorithm on single images for the SHIP DATASET 2 is significantly worse than on the SHIP DATASET 1. The nature of the SHIP DATASET 2 (camera installed on a buoy which is subject to motion, as well as the low height of the camera above the surface) makes it harder for the basic algorithm to detect the horizon and subsequently the ship. Occlusion of the ship by ocean waves in front of the camera is another reason for such performance. Without tracking part of the algorithm the detection of ships in such condition is very limited.

The worst results in tracking in video was observed on sequences where the size of the ship was small (less than 20 pixels). In that case validation range for the detection is also small and it is easier to miss the track of the ship between the frames in a presence of the strong buoy (and camera attached to it) motion or visual occlusion of the ship by the sea waves.

The dataset for visual tracking of marine vehicles contained only one or no ships present in the video. In case when multiple ships are present on the horizon performance of the tracking may suffer from target ID switch when a track initially assigned to one object may be reassigned to another detected target. However, if the ID of targets is not important and only the location of the targets needs to be reported the proposed scheme should provide results within the accuracy range shown above.

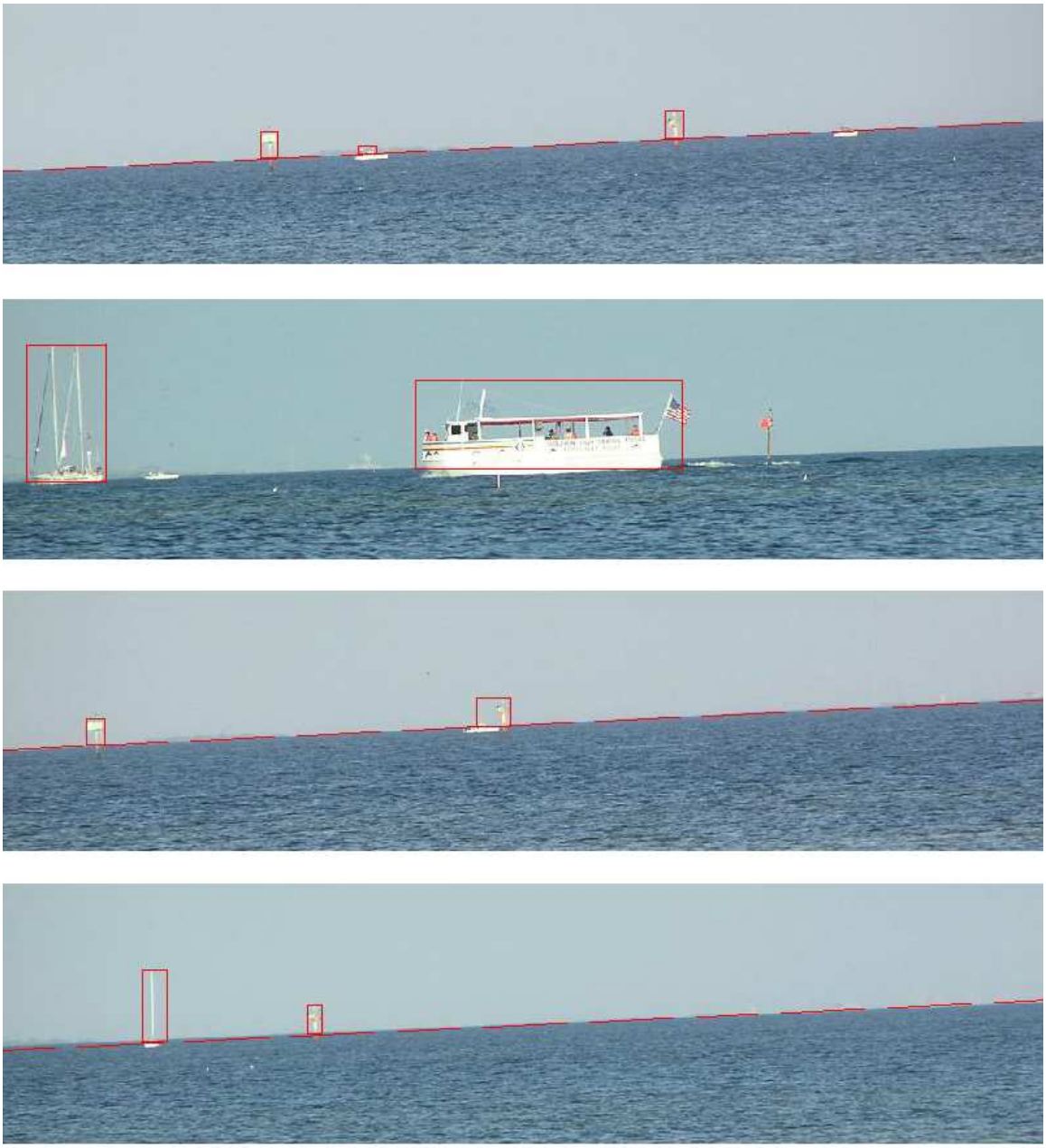

Figure 6.1. Results of marine vehicle detection in single images.

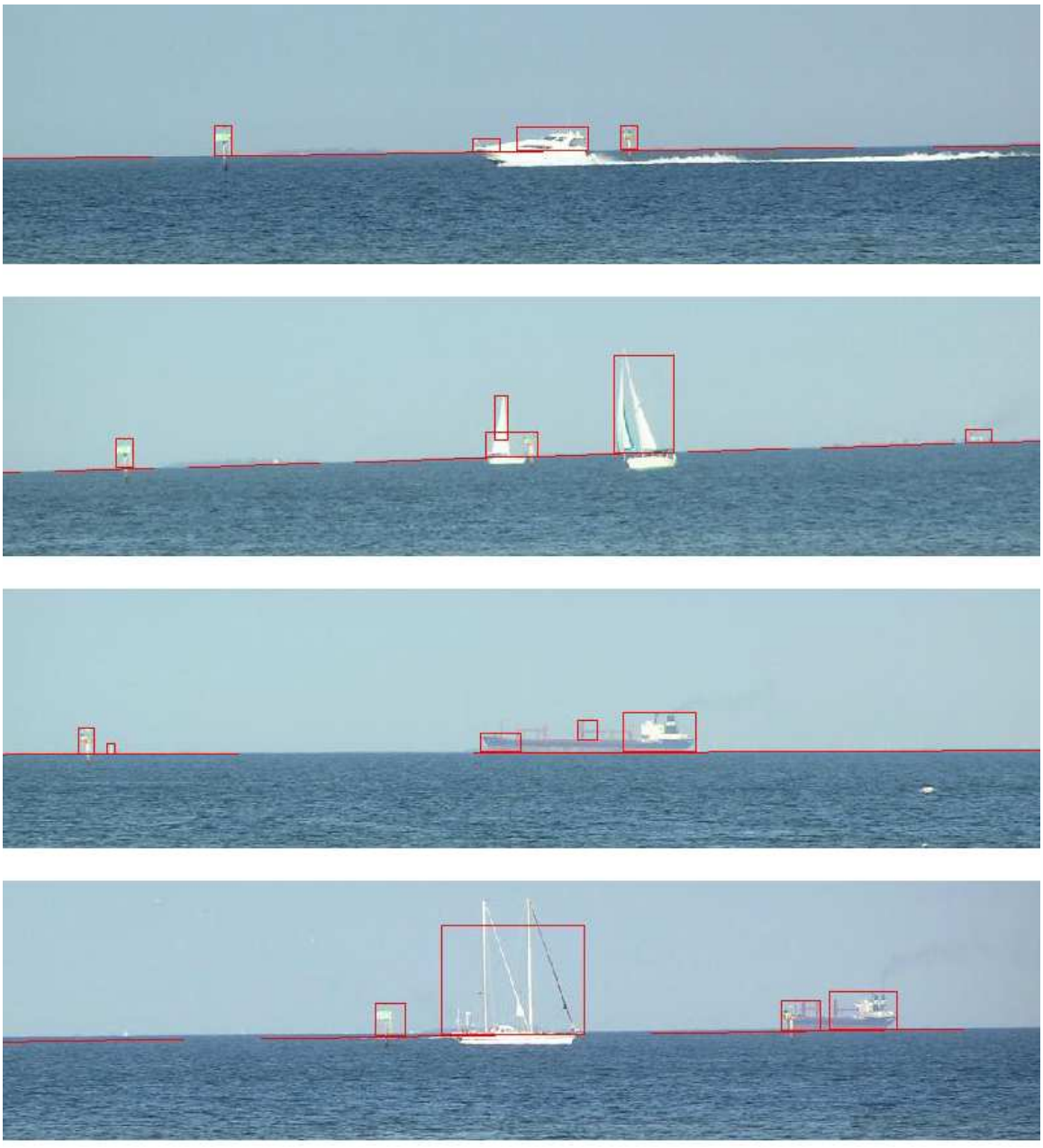

Figure 6.2. Examples of ship localization fragmentation. Some of the single-object ships were detected multiple times causing false alarms.

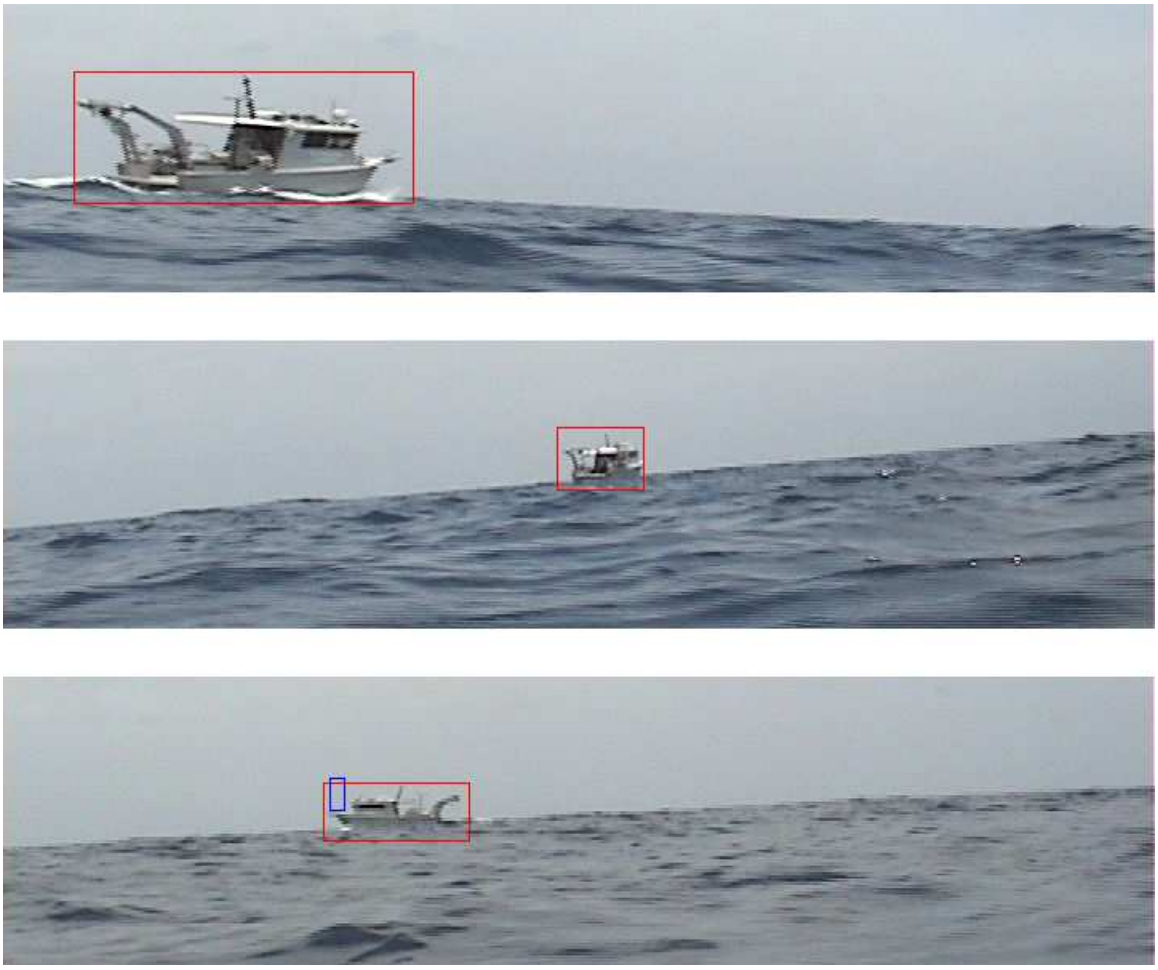

Figure 6.3. Examples of ship detection in video. The picture on the bottom shows an example of failure of detection due to temporal fragmentation of the tracks.

CHAPTER 7

CONCLUSIONS

A new technique for automatic detection and tracking of marine vehicles in images and video of open sea was presented. The proposed computer vision-based algorithm combined a horizon detection method with edge detection and postprocessing. Several datasets of still images and video sequences were used to evaluate the performance of the proposed technique. For video sequences the original algorithm was enhanced by using the Kalman filter and a tracking algorithm derived from Multiple Hypothesis Framework. Because the detection algorithm depends on accurate horizon detection, several horizon detection algorithms were evaluated for accuracy of horizon detection.

Experiments conducted on image and video data showed promising results for marine vehicle detection and tracking. High detection rate with a moderate alarm rate for low threshold values was recorded for still images. The visual results for the experiments reflect the fact that a typical failure for ship detection in a single frame occurs due to multiple region representation of single objects. This creates a miss result for the original ship and a false alarm for the attempt. The results suggest that the main cause of failures and false alarms are edge-detection and postprocessing steps in the original algorithm when a single object in the sea is represented by several disjoint regions in the postprocessed image.

The main issues with bad tracking performance are related to temporal fragmentation of tracks. Reducing temporal fragmentation of tracks may lower the false alarm rate and increase tracking accuracy in the future. Temporal fragmentation in tracking usually occurs when one track is prematurely terminated because of the long frame-range occlusion and a new track is started when the watercraft is again visually available. Introducing

recognition of objects in separate tracks may be one of the approaches to reduce such temporal fragmentation.

In future work basic noise removal and color enhancement may be applied for a more reliable horizon detection which follows image acquisition. An introduction of a training step in order to identify the parameters of the Canny edge detector may increase the initial segmentation accuracy and make it adaptable for various daylight conditions. The segmentation accuracy will be improved with an addition of "merge" procedure, which would connect closely located segments belonging to one object. One of the possible directions here is connecting intermittent lines of the contour of marine vehicles using segment finding techniques described in [44].

The current detection scheme assumes deployment of a buoy in open sea waters and coastal line was not considered to be present on the horizon. Further direction of the research may consider this, more complicated environment. Some results on maritime surveillance in coastal area can be found in [45]. Detection of marine vehicles can be also paired with marine vehicles classification. Once detected in an image or video sequence a ship can be classified into a number of categories with methods similar to those mentioned in the Chapter 1 for FLIR-based images. Determination of the distance to the target may be another desired functionality following visual detection.

REFERENCES

[1] M.I. Skolnik. *Introduction to radar systems*. McGraw-Hill New York, 1980.

[2] R. Khan, B. Gamberg, D. Power, J. Walsh, B. Dawe, W. Pearson, and D. Millan. Target detection and tracking with a high frequency ground waveradar. *Oceanic Engineering, IEEE Journal of*, 19(4):540–548, 1994.

[3] B. Root. HF radar ship detection through clutter cancellation. *Radar Conference, 1998. RADARCON 98. Proceedings of the 1998 IEEE*, pages 281–286, 1998.

[4] M. Hirota, T. Furuse, K. Ebana, H. Kubo, K. Tsushima, T. Inaba, A. Shima, M. Fujinuma, and N. Tojyo. Magnetic detection of a surface ship by an airborne LTS SQUID MAD. *Applied Superconductivity, IEEE Transactions on*, 11(1 Part 1):884–887, 2001.

[5] J.C. Curlander and R.N. McDonough. Synthetic aperture radar- Systems and signal processing(Book). *New York: John Wiley & Sons, Inc.*, 1991.

[6] M.T. Rey, J.K. Tunaley, J.T. Folinsbee, P.A. Jahans, J.A. Dixon, and M.R. Vant. Application Of Radon Transform Techniques To Wake Detection In Seasat-A SAR Images. *Geoscience and Remote Sensing, IEEE Transactions on*, 28(4):553–560, 1990.

[7] D.R. Thompson and J.R. Jensen. Synthetic aperture radar interferometry applied to ship-generated internal waves in the 1989 Loch Linnhe experiment. *Journal of Geophysical Research*, 98(C6):10259–10270, 1993.

[8] L.M. Murphy. Linear feature detection and enhancement in noisy images via the Radon transform. *Pattern Recognition Letters*, 4(4):279–284, 1986.

[9] D. Gibbins, DA Gray, and D. Dempsey. Classifying ships using low resolution maritime radar. *Signal Processing and Its Applications, 1999. ISSPA'99. Proceedings of the Fifth International Symposium on*, 1, 1999.

[10] F. Lesage and L. Gagnon. Experimenting level set-based snakes for contour segmentation in radar imagery. *Proceedings of SPIE*, 4041:154, 2000.

[11] P. Valin, Y. Tessier, and A. Jouan. Hierarchical ship classifier for airborne synthetic aperture radar (SAR) images. *Signals, Systems, and Computers, 1999. Conference Record of the Thirty-Third Asilomar Conference on*, 2, 1999.

[12] C. Yuan and D. Casasent. Composite filters for inverse synthetic aperture radar classification of small ships. *Optical Engineering*, 41:94, 2002.

[13] V. Gouaillier and L. Gagnon. Ship silhouette recognition using principal components analysis. *Proc. SPIE Conf. on Applications of Digital Image Processing XX*, 3164:59–69.

[14] C. Alippi. Real-time analysis of ships in radar images with neural networks. *Pattern Recognition*, 28(12):1899–1913, 1995.

[15] Q. Luo, TM Khoshgoftaar, and A. Folleco. Classification of Ships in Surveillance Video. *Information Reuse and Integration, 2006 IEEE International Conference on*, pages 432–437, 2006.

[16] S. Fefilatyev, D.B. Goldgof, and L. Langebrake. Towards detection of marine vehicles on horizon from buoy camera. *Proceedings of SPIE*, 6736:67360O, 2007.

[17] S. Todorovic. *Statistical Modeling and Segmentation of Sky/Ground Images*. PhD thesis, Master thesis, University of Florida, 2002.

[18] S.M. Ettinger, M.C. Nechyba, P.G. Ifju, and M. Waszak. Vision-guided flight stability and control for micro air vehicles. *Advanced Robotics*, 17(7):617–640, 2003.

[19] S. Todorovic, MC Nechyba, and PG Ifju. Sky/ground modeling for autonomous MAV flight. *Robotics and Automation, 2003. Proceedings. ICRA'03. IEEE International Conference on*, 1, 2003.

[20] S. Todorovic and MC Nechyba. A vision system for intelligent mission profiles of micro air vehicles. *Vehicular Technology, IEEE Transactions on*, 53(6):1713–1725, 2004.

[21] T. Cornall and G. Egan. Measuring Horizon Angle from Video on a Small Unmanned Air Vehicle, 2004.

[22] T. Cornall and G. Egan. Calculating Attitude from Horizon Vision. *Eleventh Australian International Aerospace Congress, Melbourne*, 2005.

[23] G.Q. Bao, S.S. Xiong, and Z.Y. Zhou. Vision-Based Horizon Extraction for Micro Air Vehicle Flight Control. *Instrumentation and Measurement, IEEE Transactions on*, 54(3):1067–1072, 2005.

[24] TG McGee, R. Sengupta, and K. Hedrick. Obstacle Detection for Small Autonomous Aircraft Using Sky Segmentation. *Robotics and Automation, 2005. Proceedings of the 2005 IEEE International Conference on*, pages 4679–4684, 2005.

[25] S. Fefilatyev, V. Smarodzinava, L.O. Hall, and D.B. Goldgof. Horizon Detection Using Machine Learning Techniques. *Machine Learning and Applications, 2006. ICMLA'06. 5th International Conference on*, pages 17–21, 2006.

[26] L. Fety, M. Terre, and X. Noreve. Image processing for the detection of the horizon and device for the implemention thereof. *United States Patent 5,214,720, Thompson TRT Defense*, 1991.

[27] B. Taylor, C. Bil, S. Watkins, and G. Egan. Horizon Sensing Attitude Stabilisation: A VMC Autopilot. *International UAV Systems Conference, Bristol, UK*, 2003.

[28] M. Sonka, V. Hlavac, and R. Boyle. Image Processing, Analysis, and Machine Vision. 2007.

[29] MC Shin, DB Goldgof, and KW Bowyer. Comparison of Edge Detector Performance through Use in an Object Recognition Task. *Computer Vision and Image Understanding*, 84(1):160–178, 2001.

[30] M. Shin, D. Goldgof, and KW Bowyer. An objective comparison methodology of edge detection algorithms using a structure from motion task. *Proceedings of CVPR*, pages 190–195.

[31] J. Canny. A computational approach to edge detection. *IEEE Transactions on Pattern Analysis and Machine Intelligence*, 8(6):679–698, 1986.

[32] R.C. Gonzalez and R.E. Woods. Digital Image Processing.

[33] R. Jain, R. Kasturi, and B.G. Schunck. *Machine vision*. McGraw-Hill, Inc. New York, NY, USA, 1995.

[34] G. Welch and G. Bishop. An Introduction to the Kalman Filter. *ACM SIGGRAPH 2001 Course Notes*, 2001.

[35] E. Cuevas, D. Zaldivar, and R. Rojas. Kalman filter for vision tracking.

[36] LC Langebrake, CE Lembke, RH Weisberg, RH Byrne, DR Russell, G. Tilbury, and R. Carr. Design and initial results of a bottom stationing ocean profiler. *Oceans'02 MTS/IEEE*, 1, 2002.

[37] S.J. Pratt. Submarine periscope systems, July 18 1989. US Patent 4,848,886.

[38] D. Reid. An algorithm for tracking multiple targets. *Automatic Control, IEEE Transactions on*, 24(6):843–854, 1979.

[39] I.J. Cox, S.L. Hingorani, et al. An efficient implementation of Reid's multiple hypothesis tracking algorithm and its evaluation for the purpose of visual tracking. *IEEE Transactions on Pattern Analysis and Machine Intelligence*, 18(2):138–150, 1996.

[40] D. Doermann and D. Mihalcik. Tools and techniques for video performance evaluation. *Pattern Recognition, 2000. Proceedings. 15th International Conference on*, 4, 2000.

[41] R Kasturi, D. Goldgof, P. Soundararajan, V. Manohar, J Garofolo, B. Bowers, M. Boonstra, V. Korzhova, and J. Zhang. Framework for Performance Evaluation of Face, Text, and Vehicle Detection and Tracking in Video: Data, Metrics, and Protocol. *IEEE Transactions on Pattern Analysis and Machine Intelligence*, page doi.ieeecomputersociety.org/10.1109/TPAMI.2008.57.

[42] C.J.C. Burges. A Tutorial on Support Vector Machines for Pattern Recognition. *Data Mining and Knowledge Discovery*, 2(2):121–167, 1998.

[43] N. Littlestone and MK Warmuth. The weighted majority algorithm. *Foundations of Computer Science, 30th Annual Symposium on*, pages 256–261.

[44] NC Rowe, LL Grewe, U.S.N.P. Sch, and CA Monterey. Change detection for linear features in aerial photographs usingedge-finding. *Geoscience and Remote Sensing, IEEE Transactions on*, 39(7):1608–1612, 2001.

[45] D.D. Morris, B.R. Colonna, and F.D. Snyder. Image-based motion stabilization for maritime surveillance. *Proceedings of SPIE*, 6497:64970F, 2007.